Short-range interactions are irrelevant at the quasiperiodicity-driven Luttinger liquid to Anderson glass transition

Miguel Gonçalves,[1] J. H. Pixley,[2,3] B. Amorim,[4] Eduardo V. Castro,[5,6] and Pedro Ribeiro[7,6]

[1]*CeFEMA-LaPMET, Departamento de Física, Instituto Superior Técnico, Universidade de Lisboa, Av. Rovisco Pais, 1049-001 Lisboa, Portugal*

[2]*Department of Physics and Astronomy, Center for Materials Theory, Rutgers University, Piscataway, New Jersey 08854, USA*

[3]*Center for Computational Quantum Physics, Flatiron Institute, 162 5th Avenue, New York, New York 10010, USA*

[4]*Centro de Física das Universidades do Minho e do Porto (CF-UM-UP), Laboratório de Física para Materiais e Tecnologias Emergentes (LaPMET), Universidade do Minho, 4710-057 Braga, Portugal*

[5]*Centro de Física das Universidades do Minho e Porto, LaPMET, Departamento de Física e Astronomia, Faculdade de Ciências, Universidade do Porto, 4169-007 Porto, Portugal*

[6]*Beijing Computational Science Research Center, Beijing 100193, China*

[7]*CeFEMA, Instituto Superior Técnico, Universidade de Lisboa, Av. Rovisco Pais, 1049-001 Lisboa, Portugal*

(Received 12 June 2023; revised 4 December 2023; accepted 4 January 2024; published 23 January 2024)

We show that short-range interactions are irrelevant around gapless ground-state delocalization-localization transitions driven by quasiperiodicity in interacting fermionic chains. In the presence of interactions, these transitions separate Luttinger liquid and Anderson glass phases. Remarkably, close to criticality, we find that excitations become effectively noninteracting. By formulating a many-body generalization of a recently developed method to obtain single-particle localization phase diagrams, we carry out precise calculations of critical points between Luttinger liquid and Anderson glass phases and find that the correlation length critical exponent takes the value $\nu = 1.001 \pm 0.007$, compatible with $\nu = 1$ known exactly at the noninteracting critical point. We also show that other critical exponents, such as the dynamical exponent z and a many-body analog of the fractal dimension are compatible with the exponents obtained at the noninteracting critical point. Noteworthy, we find that the transitions are accompanied by the emergence of a many-body generalization of previously found single-particle hidden dualities. Finally, we show that in the limit of vanishing interaction strength, all finite-range interactions are irrelevant at the noninteracting critical point.

DOI: 10.1103/PhysRevB.109.014211

I. INTRODUCTION

There has been a continued interest in the effects of quasiperiodicity on quantum many-body systems thanks to their experimental accessibility in ultracold atoms and trapped ions [1–10] and most recently moiré materials [11]. From a theoretical point of view, the effects of interactions on Anderson insulating ground states is also of paramount importance in the context of many-body localization, where random and quasiperiodic systems have important and fundamental differences that are currently under intense scrutiny [12–15]. Of paramount importance is understanding the nature of such many-body localization phase transitions that take place at finite energy density far away from the ground state [16–24]. However, even in the limit of the ground state, the nature of the universality class of the interacting quasiperiodic electronic glass transition has remained poorly understood.

A great deal of understanding has been achieved in noninteracting quasiperiodic systems thanks to rigorous results on the paradigmatic Aubry-André model [25–28], where an energy-independent delocalization-localization transition takes place, and on its generalizations to phase diagrams that contain mobility edges and/or critical phases [29–35]. However, the interplay between quasiperiodicity and interactions has been less explored. Typically, the studies on this interplay are in the context of many-body localization, for highly excited states in the middle of the many-body spectrum [16–24]. An equally interesting direction is the study of ground-state localization properties [14,15,28,36–44]. Deep enough in the localized phase, upon adding nearest-neighbor interactions to Aubry-André model, the ground state remains localized, giving rise to an Anderson glass (AG) phase [28,37,40,45]. On the other hand, at weak interaction strength the Luttinger liquid (LL) phase is stable towards the inclusion of a sufficiently weak quasiperiodic potential [40,46]. The gapless ground-state delocalization-localization transition therefore persists in the presence of interactions, corresponding to a transition between the LL and AG phases. The critical properties of the LL-AG transition were studied in detail for the noninteracting Aubry-André model [27,28,47], and it was proposed in Ref. [28] that nearest-neighbor repulsive interactions may be irrelevant at the critical point. In more generic interacting models beyond the paradigmatic Aubry-André model, the ground-state localization properties remain largely unexplored.

In this paper we show that interactions are irrelevant around quasiperiodicity-driven LL-AG transitions for a broad class of noninteracting and interacting generalizations of

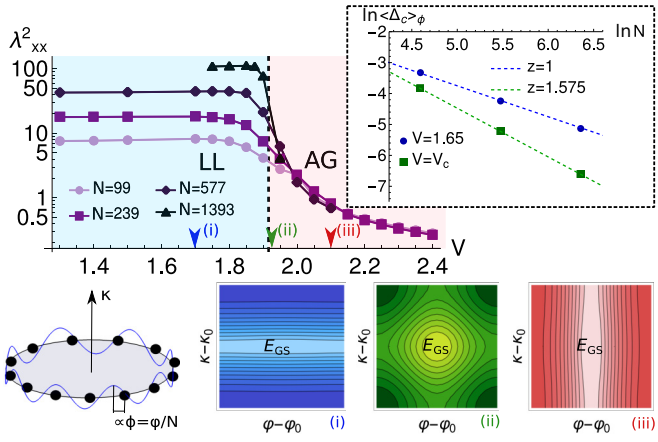

FIG. 1. Quantum phase transition between Luttinger liquid (LL) and Anderson glass (AG) phases. The variance of the position operator λ^2_{xx}, as given in Eq. (3) and computed using open boundary conditions for different system sizes N, is plotted versus the quasiperiodic potential strength V, for the model in Eq. (1) with $V_2 = 0.25, t_2 = 0.2, U = 0.5$, and $U_2 = 0.4$. The scaling of the ϕ-averaged charge gap with system size [see Eq. (4) and Fig. 4(c) for definition and additional details] in the LL phase (for $V = 1.65$) and at the critical point (indicated by the vertical dashed line) is shown in the inset, unveiling a non-Lorentz-invariant critical point (with dynamical critical exponent $z > 1$). The blue and green dashed lines show the scaling behavior known for the noninteracting Aubry-André model, respectively, at extended and critical points, which is compatible with the scaling behavior observed at the LL phase and the interacting critical point. Below these figures, we show the $E_{\rm GS}(\varphi, \kappa)$ contours for a periodic system with a threaded flux κ (illustrated in the bottom left figure), for $N = 41$, at representative points in the (a) LL and (c) AG phases, and at the (b) self-dual point that approaches the critical point (whose estimation is shown by the vertical dashed line) as $N \to \infty$. (φ_0, κ_0) in these figures is chosen so that $E_{\rm GS}(\varphi_0, \kappa_0)$ is minimum.

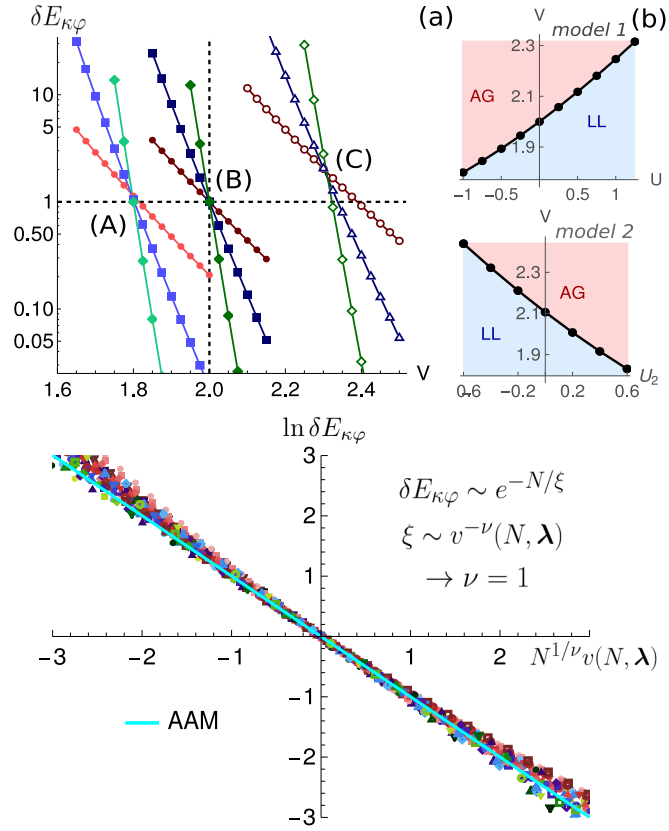

FIG. 2. (a) $\delta E_{\kappa\varphi}$ defined in Eq. (2) (using $\delta s = \pi/20$) for (A) model 1 [see main text below Eq. (1)], with $U = -1$; (B) Aubry-André model (C) model 2 with $U_2 = -0.4$, for $L = \{17(\text{red}), 41(\text{blue}), 99(\text{green})\}$. (b) Critical points for the LL to AG transition for models 1 and 2 [see definitions below Eq. (1)], estimated through the strength of the quasiperiodic potential $V = V_c(N, \boldsymbol{\lambda})$ that satisfies the self-duality condition $\delta E_{\kappa\varphi}(N, \boldsymbol{\lambda}) = 1$, for $N = 99$, where $\boldsymbol{\lambda}$ contains the model parameters. The critical point in Fig. 1 (vertical dashed line) was estimated in the same way. This estimation assumes that $V_c(N = 99, \boldsymbol{\lambda}) \approx V_c(\infty, \boldsymbol{\lambda})$. Its validity is confirmed by the small error bars (smaller or of the size of the data points), computed through $|V_c(99, \boldsymbol{\lambda}) - V_c(41, \boldsymbol{\lambda})|$. (c) Data collapse of $\ln\delta E_{\kappa\varphi}$ as a function of $N^{1/\nu} v(N, \boldsymbol{\lambda})$, using $\nu = 1$, where $v(N, \boldsymbol{\lambda}) = [V - V_c(N, \boldsymbol{\lambda})]/V_c(N, \boldsymbol{\lambda})$. The data was obtained across all the LL-AG transitions shown in (b). The results for $N = \{17, 41, 99\}$ correspond to the red, blue and green markers, respectively. In cyan, we show the result for the noninteracting Aubry-André model.

the Aubry-André model, which include next-nearest-neighbor hoppings and interactions and an additional quasiperiodic potential. In particular, we show that the excitations become effectively noninteracting around these transitions and provide solid evidence that the addition of interactions does not affect any of the (infinite number of) critical exponents obtained in the noninteracting limit, although they modify nonuniversal properties, e.g., the location of the critical point. Remarkably, we also find that many-body generalizations of the single-particle dualities discovered for widely different one-dimensional (1D) models [30,34,48] emerge around criticality. We present a scaling argument based on the perturbative effects of interactions at the Aubry-Andre critical point, which demonstrates that short-range interactions are irrelevant. The same argument shows that long-range interactions can become relevant.

Our main results are shown in Figs. 1, 2. In Fig. 1 we show an example of a LL-AG transition, in which we set all the couplings of our class of models [in Eq. (1) below] different from zero. A way to capture this transition is with the variance of the position operator [see Eq. (3) for definition] [49–51] that diverges (saturates) at the LL (AG) phase due to the extended (localized) nature of the many-body wave function.

One of our main findings in this work is that this transition can also be captured in a precise manner with minimal scaling assumptions, using a many-body generalization of the single-particle theory developed in Refs. [48,52]. This involves considering periodic approximations of the quasiperiodic system, as illustrated at the bottom left corner of Fig. 1, and inserting a flux κ through the resulting ring. The localization properties can then be inferred based on how the ground-state energy ($E_{\rm GS}$) depends on these fluxes and on real-space shifts between the lattice and origin of the potential that we encode in the variable φ, as illustrated in Fig. 1(a), as the size of the periodic approximation (N) is increased. The quasiperiodic limit is approached for $N \to \infty$. In Fig. 1, we show examples of the energy contours for fixed $N = 41$, for different values

of V. We can see that in the LL (AG) phase, there is a very small dependence on φ (κ), while close to the critical point, there is an equal dependence on both phases. We can make a more quantitative analysis by computing the ratio between the energy dispersions along κ and φ, respectively, $\delta E_{\kappa\varphi}$ [see Eq. (2) for precise definition], for different N. Example results are given in Fig. 2(a) for different models, where we can see that $\delta E_{\kappa\varphi}$ diverges (scales to zero) at the LL (AG) phase. This implies that the $\varphi(\kappa)$ dependence becomes irrelevant with respect to the $\kappa(\varphi)$ dependence at the LL (AG) phases as N increases, and the model flows to a delocalized (localized) fixed point as defined in Ref. [52]. Remarkably, at the critical point, $\delta E_{\kappa\varphi}$ approaches unity as N is increased, which implies that the shift and flux dependencies become equivalent. The self-dual point, defined here as the point for which $\delta E_{\kappa\varphi} = 1$,[1] therefore approaches the critical point as $N \to \infty$, providing a very precise way of estimating it.

With the ansatz $\delta E_{\kappa\varphi} \propto e^{-N/\xi}$, where $\xi \sim |V - V_c|^{-\nu}$ is the correlation length, we were able to collapse the results for each model considered here into a single universal curve using the correlation length critical exponent $\nu = 1$ known for the noninteracting Aubry-André model, as shown in Fig. 2(c). The obtained scaling function near criticality is in excellent agreement with the one obtained for the noninteracting Aubry-André model, shown in cyan in Fig. 2(c). The good quality of the collapse and further results on additional critical exponents presented throughout the paper support the conclusion that around criticality, different interacting and noninteracting models belong to the same noninteracting universality class.

II. MODELS AND METHODS

We study the class of models described by the Hamiltonian

$$\begin{aligned} H = &-t\sum_i c_i^\dagger c_{i+1} - t_2\sum_i c_i^\dagger c_{i+2} + \text{H.c.} \\ &+ \sum_i (V\cos(2\pi\tau i + \phi) + V_2\cos[2(2\pi\tau i + \phi)])c_i^\dagger c_i \\ &+ U\sum_i n_i n_{i+1} + U_2\sum_i n_i n_{i+2}, \end{aligned} \tag{1}$$

where $c_i^\dagger$ creates a particle at site i and we set $t = 1$ throughout the paper. The first and third rows contain nearest- and next-nearest-neighbor hoppings and interactions, respectively, while the second row contains quasiperiodic potentials of intensity V and V_2, with τ being an irrational number and the phase ϕ representing a shift of the potentials with respect to the lattice sites. For the results presented in this paper, we set $\tau = 1/\sqrt{2}$ (to compare results with Refs. [28,40]) and work at half-filling $\rho = 1/2$ (unless otherwise specified), choosing a number of particles $N_p = \lfloor N/2 \rfloor$, where $\lfloor x \rfloor$ denotes the integer part of x (the floor function). We have checked that our conclusions do not rely on being at this particular filling, see Appendix B. We choose the following sets of parameters: Aubry-André model with nearest-neighbor interaction, $V_2 = t_2 = U_2 = 0$ (model 1); generalized Aubry-André model, with $U = 0.5, V_2 = 0.25, t_2 = 0.2, U_2 \neq 0$ (model 2).

To study the models in detail, we computed several different quantities using the DMRG technique [53,54], as implemented in the ITENSOR library [55,56], applying both periodic and open boundary conditions. We required ITENSOR's truncation error to be less than 10^{-10} and only stopped the sweeping procedure once some convergence requirements were satisfied, up to a maximum of 500 sweeps. In particular, for twisted boundary conditions, we require the energy variance, $\Delta_H = \langle H^2\rangle - \langle H\rangle^2$, to be below 5×10^{-6}; the ground-state energy difference between two sweeps to be below $\Delta E_{\text{GS}} = 10^{-5}$; and the difference in the entanglement entropy at the middle bond inbetween two sweeps to be below $\Delta S_{\text{GS}} = 10^{-3}$. For open boundary conditions, we require Δ_H at least below 10^{-6}, $\Delta E_{\text{GS}} \leqslant 10^{-7}$, and $\Delta S_{\text{GS}} \leqslant 10^{-4}$.

In our finite-size simulations, we use rational approximants of τ, $\tau_c = p/N$, with p and N coprime numbers. These approximants were chosen to be exact convergents of the continued fraction expansion of τ.

III. TWISTED BOUNDARY CONDITIONS

We consider a ring with N sites as illustrated in the bottom left corner of Fig. 1 with twisted boundary conditions that corresponds to threading a flux κ through the system. This flux can simply be added to the model in Eq. (1) by making the replacement $t \to te^{ik}$ and $t_2 \to t_2 e^{2ik}$, with $k = \kappa/N$. For the choices $\tau = \tau_c$, making shifts $\phi \to \phi + 2\pi/N$ simply corresponds to a relabeling of the indices in this model [48], which implies that the many-body ground-state energy is periodic in ϕ with period $\Delta\phi = 2\pi/N$. With this in mind, we define the rescaled variable $\varphi = N\phi$ so that $E_{\text{GS}}(\varphi, \kappa)$ has a period $\Delta\varphi = 2\pi$. We define the flux-shift sensitivity, $\delta E_{\kappa\varphi}$, as

$$\delta E_{\kappa\varphi} = \lim_{\delta s \to 0} \frac{E_{\text{GS}}(\varphi_0, \kappa_0 + \delta s) - E_{\text{GS}}(\varphi_0, \kappa_0)}{E_{\text{GS}}(\varphi_0 + \delta s, \kappa_0) - E_{\text{GS}}(\varphi_0, \kappa_0)}, \tag{2}$$

where (φ_0, κ_0) are defined so that $E(\varphi_0, \kappa_0)$ is minimum to ensure that $\delta E_{\kappa\varphi} = 1$ at self-dual points.[2] Note that the values of (φ_0, κ_0) can depend on N and on the number of particles N_p. For the system sizes used in the calculations with periodic boundary conditions and $N_p = \lfloor N/2 \rfloor$, we found $(\varphi_0, \kappa_0) = (0, \pi)$ for $N = 17, 41$ and $(\varphi_0, \kappa_0) = (\pi, 0)$ for $N = 99$. $\delta E_{\kappa\varphi}$ is the many-body generalization of a similar quantity already introduced for the single-particle eigenenergies of noninteracting quasiperiodic models in Ref. [48]. In the LL (AG) phase, we expect $\delta E_{\kappa\varphi} \to \infty$ ($\delta E_{\kappa\varphi} \to 0$) for increasing N. At the critical point, we have $\delta E_{\kappa\varphi} \to 1$, as we will see. The flux-shift sensitivity has some similarities with the Drude weight/superfluid fraction [57]. However, the latter only measures the variation of the ground-state energy with respect to the flux κ, therefore missing important information on the duality between κ and φ that exists for the models here studied.

[1] This matches the usual definition of a self-dual point, when an exact duality transformations can be explicitly constructed.

[2] Note that (φ_0, κ_0) should be chosen so that at self-dual points, the energy dispersions are invariant under switching φ-φ_0 and κ-κ_0.

It is clear from the $E_{\rm GS}(\varphi,\kappa)$ contour plots in Fig. 1 that there is a duality between the LL and AG phases around criticality under switching $(\varphi\text{-}\varphi_0)$ and $(\kappa\text{-}\kappa_0)$. The critical point is the self-dual point of this duality, in which $E_{\rm GS}$ is invariant under this exchange. In Ref. [48] we have uncovered similar dualities in the single-particle case and found that they could be traced back to hidden duality transformations between the single-particle wave functions. Remarkably, in the presence of interactions, a many-body generalization of these duality transformations can still be formulated. In Appendix D we provide the precise definition and some examples.

IV. OPEN BOUNDARY CONDITIONS

We also employ open boundary conditions that allow us to reach fairly large system sizes [55,56]. In order to carry out a complete study of the LL and AG phases, and of the transition between them, we compute several quantities that we detail below.

The variance of the position operator shown in Fig. 1 can be defined as [49–51]

$$\lambda_{xx}^2 = (\langle\Psi|\,\hat{x}^2\,|\Psi\rangle - \langle\Psi|\,\hat{x}\,|\Psi\rangle^2)/N_p, \tag{3}$$

where $\hat{x} = \sum_{i=1}^{N_p}\hat{x}_i = \sum_{i=1}^{N} x_i c_i^\dagger c_i$ is the many-body position operator and N_p is the number of particles. Since it measures the variance of the position operator, it can distinguish between the LL and AG phases: it diverges (saturates) with N, due to the extended (localized) nature of the many-body wave function at the LL (AG) phase.

To verify the gapless nature of the transition and obtain the dynamical critical exponent z, we also computed the charge gap, defined as

$$\Delta_c = E_{\rm GS}(N_p+1) + E_{\rm GS}(N_p-1) - 2E_{\rm GS}(N_p) \sim N^{-z}, \tag{4}$$

where $E_{\rm GS}(N_p)$ is the ground-state energy for N_p particles.

In order to study the scaling of the entanglement in different regions of the phase diagram, we computed the entanglement entropy [58,59], defined as

$$\mathcal{S} = -{\rm Tr}[\rho_{\rm A}\ln\rho_{\rm A}],\ \ \rho_{\rm A} = {\rm Tr}_{\rm B}\,|\psi\rangle\,\langle\psi|\,, \tag{5}$$

where we choose the partition A containing the first N_A sites of the chain. For a 1D critical system whose continuum limit is a conformal field theory with central charge c, we have that [60]

$$\mathcal{S} = \frac{c}{6}\ln\left(\frac{N}{\pi}\sin(\pi N_A/N)\right) + C'. \tag{6}$$

This is the expected behavior at the LL phase (with $c=1$), while at the AG phase, $\mathcal{S}$ becomes nonextensive for large enough N_A.

To better understand the nature of single-particle excitations we also introduce here the particle-addition correlation matrix, that we define as

$$C_e^{ij} = \langle c_i^\dagger c_j\rangle_{N_p} - \langle c_i^\dagger c_j\rangle_{N_p-1}, \tag{7}$$

where $\langle\rangle_{N_p}$ denotes expectation value in the ground-state with N_p particles. The eigenvalues and eigenvectors of the particle-addition correlation matrix, $\boldsymbol{C}_e\,|\alpha\rangle = \delta\bar{n}_\alpha\,|\alpha\rangle$, with $\alpha = 0,\ldots,N-1$, correspond to the occupations and natural orbitals. For a noninteracting system, only a single natural orbital corresponding to the N_pth highest-energy single-particle eigenstate labeled as $|\alpha=0\rangle$ is occupied (we have $\delta\bar{n}_0 = 1; \delta\bar{n}_{\alpha>0} = 0$). In contrast, in the presence of interactions, a particle that is added to the system redistributes over different natural orbitals. Therefore, the deviations from the expected behavior of a noninteracting particle can be quantified by inspecting the occupations $\{\delta\bar{n}_\alpha\}$. For this purpose, we introduce the occupation inverse participation ratio defined as $P(\{\delta\bar{n}_\alpha\}) = (\sum_\alpha |\delta\bar{n}_\alpha|^2)^{-2}\sum_\alpha |\delta\bar{n}_\alpha|^4$. For a noninteracting (interacting) particle, $P(\{\delta\bar{n}_\alpha\}) = 1$ ($P(\{\delta\bar{n}_\alpha\}) < 1$). We therefore expect that $P(\{\delta\bar{n}_\alpha\})$ should approach unity whenever interactions become irrelevant.

The nature of the low-energy excitations can also be inspected by analyzing the long wavelength (small q) behavior of the static structure factor defined as $S(q) = N^{-1}\sum_{j,l}[\langle n_j n_l\rangle - \langle n_j\rangle\langle n_l\rangle]e^{iq(j-l)}$. In the LL phase, the Luttinger liquid correlation parameter K can be computed through[3] $K = 2\pi\lim_{q\to 0} S(q)/q$ [61–64]. In a gapless noninteracting and translationally invariant system, it is easy to show that $K=1$. Inside an (interacting) LL phase, however, $K \neq 1$ in general.

To inspect the localization properties of the many-body wave function, we also computed inverse participation ratios (IPR) [65] for the density fluctuations $\delta n_i \equiv C_e^{ii}$ and for the most occupied (with $\delta\bar{n}_\alpha$ closest to 1) natural orbital that we write as $|\alpha=0\rangle = \sum_i \psi_i^{(0)}\,|i\rangle$, where $|i\rangle = c_i^\dagger\,|0\rangle$ and $|0\rangle$ is the vacuum:

$$\begin{aligned}{\rm IPR}(\{\delta n_i\}) &= \left(\sum_i |\delta n_i|\right)^{-2}\sum_i |\delta n_i|^2\\ {\rm IPR}_{\rm NO}(q) &= \left(\sum_i |\psi_i^{(0)}|^2\right)^{-q}\sum_i |\psi_i^{(0)}|^{2q}.\end{aligned} \tag{8}$$

In the noninteracting limit it is easy to show that $\delta n_i = |\psi_i^{N_p}|^2$ and $\psi_i^{(0)} = \psi_i^{N_p}$, where $\psi_i^{N_p}$ is the amplitude of the N_pth single-particle wave function (ordered by increasing eigenenergy) at site i. The quantities in Eq. (8) are therefore many-body generalizations of the single-particle IPR [66] used to study the localization properties of single-particle eigenstates. For the conventional definition of the IPR [with $q=2$ in Eq. (8)], we have IPR $\sim N^{-D_2}$, where D_2 is the fractal dimension, with $D_2 = 1$ for delocalized states, $D_2 = 0$ for localized states and $0 < D_2 < 1$ for critical states. For the generalized version, with $q \neq 0$, we have IPR $\sim N^{-\tau(q)}$, with $\tau(q) = D_q(q-1)$ and $D_q = d$ (with d the system's dimension) for fully delocalized single-fractal states, while D_q is a nonlinear function of q for multifractal states.

V. UNIVERSAL DESCRIPTION AROUND CRITICALITY

As we previously stated, Fig. 2 shows that the results for the quantity $\delta E_{\kappa\varphi}$ in significantly different models can be collapsed into a single universal scaling function. To obtain

[3]Note that the factor of 2 is needed since we are working with spinless fermions.

TABLE I. System size approximants of $\tau = 1/\sqrt{2}$ used for the finite-size calculations.

N	17	41	99	239	577	1393	∞
τ_c	$\frac{12}{17}$	$\frac{29}{41}$	$\frac{70}{99}$	$\frac{169}{239}$	$\frac{408}{577}$	$\frac{985}{1393}$	$\frac{1}{\sqrt{2}}$

the collapse in Fig. 2(c), we first defined the normalized distance to the critical point $v(N, \boldsymbol{\lambda}) = [V - V_c(N, \boldsymbol{\lambda})]/V_c(N, \boldsymbol{\lambda})$, where $\boldsymbol{\lambda} = (V_2, t_2, U, U_2)$ contains the model parameters (other than V) and $V_c(N, \boldsymbol{\lambda})$ is the value of V at the self-dual point $[\delta E_{\kappa\varphi}(N, V, \boldsymbol{\lambda}) = 1]$. The reason why we use $V_c(N, \boldsymbol{\lambda})$ and not $V_c \equiv V_c(\infty, \boldsymbol{\lambda})$ is that for smaller systems there can be some dependence of $V_c(N, \boldsymbol{\lambda})$ on N. Such dependence can arise not only from finite-size effects, but also because increasing N also slightly modifies the filling $\rho = N_p/N$ (due to N being odd) and the value of τ_c (see Table I in Appendix A).

Further assuming that

$$\delta E_{\kappa\varphi} \sim e^{-N/\xi} \tag{9}$$

with $\xi \sim v^{-\nu}(N, \boldsymbol{\lambda})$ and extracting ν from a fit using all the obtained data points, we get a critical exponent $\nu = 1.001 \pm 0.007$ (see Appendix A). Therefore, we set $\nu = 1$ and obtain an excellent collapse shown in Fig. 2(c), around the critical point, i.e., around $v(N, \boldsymbol{\lambda}) = 0$. In Appendix A we also show that this collapse is not a special feature of half-filling by also considering the case $\rho = 1/3$. We conjecture that the collapse should be observed for any filling that is not commensurate with τ as defined in Ref. [28], i.e., that does not satisfy $\rho = \text{mod}\ (n\tau_c, 1)$, with n an integer that does not depend on system size. At such commensurate fillings, single-particle gaps are opened for any strength of the quasiperiodic potential.

VI. NONINTERACTING EXCITATIONS AND ADDITIONAL CRITICAL EXPONENTS

We have seen from the quantity $\delta E_{\kappa\varphi}$ in Eq. (2) that the effects of interactions on the scaling function and ν are irrelevant. We now show that particles become effectively noninteracting in this regime and that the critical properties obtained at different critical points are identical. For the results that follow, we use open boundary conditions.

In Fig. 3(a), we show that the occupation inverse participation ratio approaches 1 around the critical point. This implies that the single-particle gapless excitations acquire a noninteracting nature. The same conclusion can be drawn by inspecting the behavior of the Luttinger parameter K, in Fig. 3(b). At small V, K does not vary significantly (note that when $V = 0$, K is known exactly for model 1 [61]). On the other hand, as V gets closer to the critical point, K approaches the noninteracting value $K = 1$. Exactly at the different critical points, the system is no longer a LL and at small q we find log-periodic corrections $S(q) \approx 0.7q[1 + a\sin(b\ln q + \alpha)]$ (see Appendix C). In the AG phase, $S(\delta q)/\delta q$, computed for the smallest nonvanishing momentum δq, decreases since $S(q) \sim q^2$ when $q \to 0$ [see Appendix C for explicit plots of $S(q)$]. In Appendix C we also show an example for attractive interactions, in which case $K > 1$ for model 1 with $V = 0$, in the Luttinger liquid phase. In this case, K decreases with increasing V and approaches 1 close to the critical point, just before $S(q)$ again acquires the universal critical behavior, at the critical point.

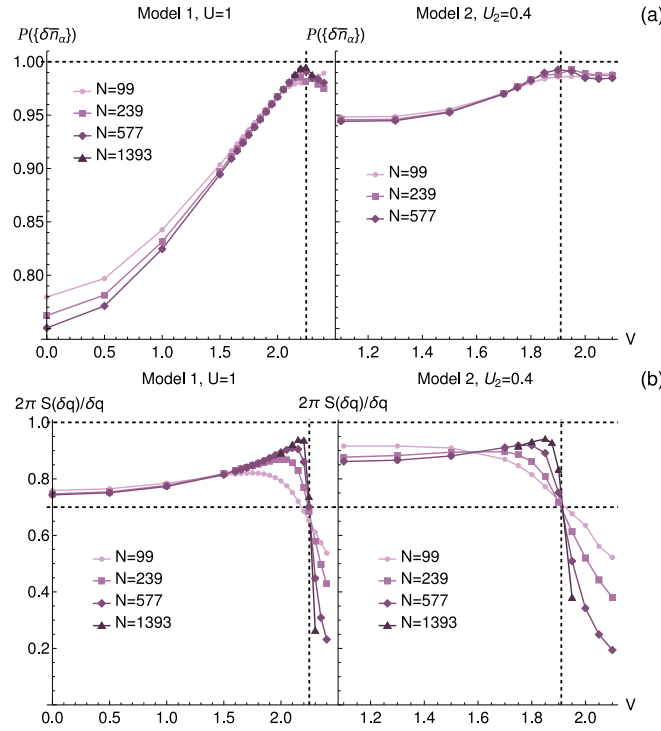

FIG. 3. Noninteracting excitations at the critical point. (a) Occupation inverse participation ratio $P(\{\delta\bar{n}_\alpha\})$ defined below Eq. (7), and (b) slope of structure factor $S(\delta q)$ for $\delta q = 20\pi/N$ as a function of V for model 1 with $U = 1, \phi = 1.123$ (left) and model 2 with $U_2 = 0.4$ (right). The vertical dashed line corresponds to the critical point estimated from $\delta E_{\kappa\varphi}$ and the horizontal dashed line is the slope of the linear contribution to $S(q)$ at the critical point (see text).

In Fig. 4(a) we show a representative example of the quantities $N\,\text{IPR}(\{\delta n_i\})$ and $N\,\text{IPR}_{\text{NO}}$ across the LL-AG transition. We observe LL (AG) phase is characterized by $\text{IPR}(\{\delta n_i\})$, $\text{IPR}_{\text{NO}} \sim N^{-1}$ (∼const.), which is confirmed by the collapse (divergence) of the curves below (above) the transition for different N, in direct analogy with the results for the single-particle IPR in the noninteracting case. Note that both quantities become almost quantitatively equal close to the critical point and at the AG phase. At the critical point we expect multifractal scaling with an infinite set of critical exponents (i.e., the multifractal spectrum). Averaging our results over ϕ, we compute the exponent τ_q defined in Eq. (8), which we show in Fig. 4(b). In this figure, we can see that in the LL phase (P_1^e and P_2^e), $D_q \approx 1$, while at interacting critical points (P_2^c and P_4^c) we observe a multifractal behavior quantitatively compatible with the one obtained at the noninteracting critical points (P_1^c and P_3^c), that is, $D_q \approx 1 - 0.227q$.[4] In Appendix C, we show explicit data for $\langle \text{IPR}_{\text{NO}}(q)\rangle_\phi$ as a function of N, from which the exponents $\tau(q)$ were extracted.

[4]By fitting to the behavior $D_q = c_1 + c_2 q$, we obtained $c_1 = 0.992 \pm 0.005$ and $c_2 = -0.227 \pm 0.004$ at the critical point of the noninteracting Aubry-André model.

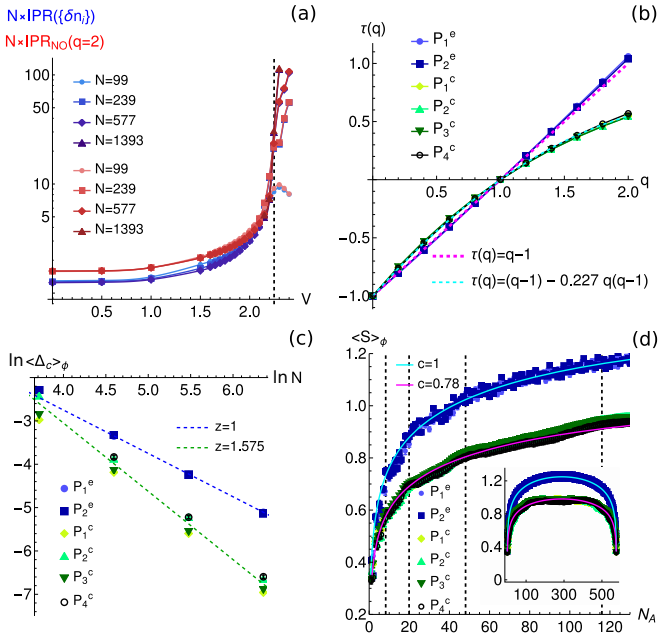

(e)

P_1^e	P_2^e	P_1^c	P_2^c	P_3^c	P_4^c
Model 1 (LL) U=1, V=2	Model 2 (LL) U_2=0.4, V=1.65	Model 1 (Crit.) U=0, V=2	Model 1 (Crit.) U=1, V=V_c	Model 2 (Crit.) U=U_2=0, V=V_c	Model 2 (Crit.) U_2=0.4, V=V_c

FIG. 4. (a) $N\mathrm{IPR}(\{\delta n_i\})$ and $N\mathrm{IPR}_{\mathrm{NO}}$ as a function of V for $U = 1, \phi = 1.123$ and $V_2 = t_2 = U_2 = 0$. The vertical dashed line shows the critical point estimated from $\delta E_{\kappa\varphi}$. (b) Exponent $\tau(q)$ defined in Eq. (8) for different models with chosen parameters indicated in table (e), where $P_i^e(P_i^c)$ denote extended (critical) points. In table (e), V_c corresponds to the estimated critical point. $\tau(q)$ was computed from linear fits to data points $(\ln N, \langle \mathrm{IPR}_{\mathrm{NO}}(q)\rangle_\phi)$, where $\langle\rangle_\phi$ denotes an average over different choices of ϕ. We took $\phi_j = 2\pi j/N_c$, $j = 0, \ldots, N_c - 1$ and $N_c \in [100\text{–}300]$. We used system sizes $N \in \{99, 239, 577\}$ for (interacting) points $P_1^e, P_2^e, P_2^c, P_4^c$ and $N \in \{99, 239, 577, 1393\}$ for (noninteracting) points P_1^c, P_3^c. (c), (d) $\langle\Delta_c\rangle_\phi$ and $\langle\mathcal{S}(N_A)\rangle_\phi$ computed by employing the same averaging procedure used in (b). In (c), the blue and green dashed lines show the scaling behavior in the noninteracting Aubry-André model, respectively, at extended and critical points. In (d), the calculation is done for $N = 577$. The main figure shows a closeup at smaller N_A, while the inset shows the results for all possible N_A. The vertical dashed lines are guides to the eye for the maxima of the log-periodic oscillations, given by $N_A^{(n)} = 116/p^n$, with $n = 0, 1, 2, 3$ and $p = \lim_{m\to\infty} N_m/N_{m+1} = 1 + \sqrt{2}$. The magenta and cyan curves correspond to fits to Eq. (6) with $c = 1$ and $c = 0.78$, respectively.

We also computed the ϕ-averaged scaling of the charge gap Δ_c in Fig. 4(c), which allowed us to extract dynamical critical exponents z. Remarkably, the scaling exponents are compatible with the exponents obtained for the noninteracting Aubry-André model. This, together with the multifractal analysis, is a strong indication that the universality class of the delocalization-localization transition is unchanged upon the addition of interactions. An important remark is that, as seen in Ref. [28], the dynamical exponent for the noninteracting Aubry-André model can depend on ρ and τ. Since here we are fixing the latter, a natural question is whether the independence of the critical exponents on the model is a special feature of our choice. In Appendix F, we argue that this is not the case by obtaining compatible finite-size scalings of the charge gap at critical points of different noninteracting models for other choices of ρ and τ.

Finally, we also plot the ϕ-averaged entanglement entropy as a function of the size of bipartition A, N_A, in Fig. 4(d). In the LL phase, S follows the behavior of Eq. (6) with $c = 1$, as in the noninteracting delocalized case [67]. At the critical point, the results are compatible with the noninteracting Aubry-André model result, showing corrections to Eq. (6) in the form of log-periodic oscillations, similarly with what was observed for critical aperiodic spin chains in Ref. [68] (see Appendix C for more detailed analysis of the log-periodic oscillations). A fit to Eq. (6) neglecting these corrections yields $c \approx 0.78$, in agreement with Ref. [69] (note, however, that in this case c cannot be interpreted as a central charge).

VII. GENERALIZED CHALKER SCALING AND IRRELEVANCE OF GENERIC SHORT-RANGE INTERACTIONS

We now provide a framework to understand why the short-range interactions we have studied so far are irrelevant. Our argument relies on a tree-level scaling analysis of the interaction at the critical point of the Aubry-André model. For completeness, we extend our discussion to long-range interactions, of the form r^{-w} with $w > 1$, and show there is a critical power law, w_c, where they eventually become relevant. We employ twisted boundary conditions and choose the long-range interaction to be a periodized form of the power-law potential $U\sum_{r,j} j^{-w} n_r n_{r+j}$, given by $U\sum_{j=1}^{N-1} N^{-w}\zeta(w, j/N)\sum_{r=1}^{N} n_r n_{r+j}$, where $\zeta(w, y) = \sum_{k=0}^{\infty}(k + y)^{-w}$ is the Hurwitz zeta function and $n_r = n_{r+N}^\dagger$ due to twisted boundary conditions. To compute the scaling dimension of the interaction term, denoted as $D_U(w)$, we write the interacting Hamiltonian on the single-particle eigenbasis of the noninteracting Aubry-André model Hamiltonian, H_0. We label single-particle states with Greek indices, $|\alpha\rangle$, and single-particle energies by ϵ_α. In this base

$$H = \sum_\alpha \epsilon_\alpha c_\alpha^\dagger c_\alpha - \sum_{\alpha,\beta,\gamma,\delta} \bar{V}_{\alpha\beta\gamma\delta} c_\alpha^\dagger c_\beta^\dagger c_\gamma c_\delta, \tag{10}$$

where $\bar{V}_{\alpha\beta\gamma\delta}$ is the antisymmetrized version of the interaction tensor in the eigenbasis of the Aubry-André model

$$V_{\alpha\beta\gamma\delta} = \frac{U}{N^w}\sum_{r=1}^{N}\sum_{j=1}^{N-1}\zeta\left(w, \frac{j}{N}\right)\langle\alpha|r\rangle\,\langle\beta|r+j\rangle\,\langle r|\gamma\rangle\,\langle r+j|\delta\rangle \tag{11}$$

with $\langle\alpha|r\rangle = \langle 0|\, c_\alpha c_r^\dagger\,|0\rangle$.

The leading contributions to the interacting term come from states with energies around the Fermi level, E_F. In the following, we denote by ϵ_0 the energy closest to E_F and we set $\epsilon_0 = 0$ for convenience. By the antisymmetry of V, the lowest-order nonvanishing contributions involve setting two indices to the Fermi level and varying the remaining, i.e., $\bar{V}_{\alpha 0\beta 0}$. Among those, we find that the dominant contribution arises for $\alpha = \beta$ (see Appendix E) and thus we may restrict our analysis to an interaction tensor of the form $\bar{V}_{0\alpha 0\alpha}$ for small $|\epsilon_\alpha|$.

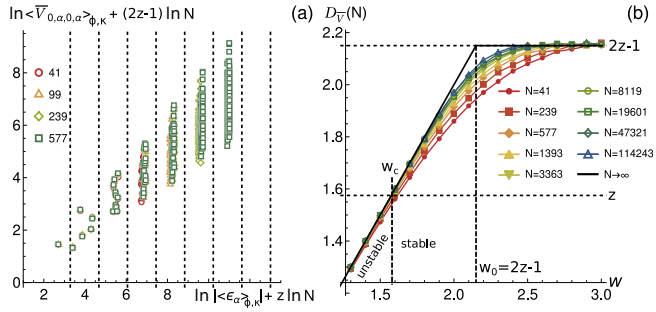

FIG. 5. Scaling dimension of long-range interactions. (a) Collapses of $\langle \bar{V}_{0\alpha 0\alpha} \rangle_{\phi,\kappa}$ calculated at the critical point of the half-filled Aubry-André model ($V = 2$) for $\tau = 1/\sqrt{2}$ (that has $z = 1.575$), for different system sizes and different energies, and for power-law interactions with decay exponent $w = 3$. Twisted boundary conditions are used and the results are averaged over 200 random configurations of ϕ and κ, denoted by $\langle\rangle_{\phi,\kappa}$. (b) Finite-size results for $D_{\bar{V}}(N, w)$. The dashed lines indicate $D_{\bar{V}} = z$ and $D_{\bar{V}} = 2z - 1$. The black lines indicate the expected thermodynamic-limit behavior. w_c corresponds to the critical value of the exponent w below which interactions become relevant.

For the chosen model (half-filling, with $\tau = 1/\sqrt{2}$), the critical point of the (noninteracting) Aubry-André model under a discrete scale transformation $r \to Nr$ is invariant under the rescaling $\epsilon_\alpha \to N^z \epsilon_\alpha$. The interacting term transforms as $\bar{V}_{0\alpha 0\alpha} \to N^{D_{\bar{V}}(w)} \bar{V}_{0\alpha 0\alpha}$, where $D_{\bar{V}}$ is the scaling dimension of the interaction tensor that can be obtained by the data collapse illustrated in Fig. 5(a). In this example, we take the half-filled Aubry-André model with $\tau = 1/\sqrt{2}$, that has $z = 1.575$, and set $w = 3$, finding that $D_{\bar{V}}(w = 3) = 2z - 1$. The relation between the energy, ϵ_α, and the interaction strength, $\bar{V}_{0\alpha 0\alpha}$, follows a generalized Chalker scaling [70–74]. However, a significant difference to previous Chalker scaling analyses is the full antisymmetrization of the interaction term that follows from fermionic statistics.

By power counting, we find the scaling dimension of the interaction to be $D_U = z - D_{\bar{V}}$, implying that interactions are irrelevant if $D_{\bar{V}} > z$ (see Appendix E for details). To infer $D_{\bar{V}}(w)$ in the thermodynamic limit, we studied the finite-size dimension $D_{\bar{V}}(w, N_m)$ (where m labels the order of the approximant size N_m), which satisfies $D_{\bar{V}}(w, \infty) \equiv D_{\bar{V}}(w)$, and can be computed through $D_{\bar{V}}(w, N_m) = -(\ln N_{m+1} - \ln N_m)^{-1}[\ln \bar{V}^{m+1}_{0101}(w) - \ln \bar{V}^{m}_{0101}(w)]$, as depicted in Fig. 5(b). As for the case $w = 3$ shown in Fig. 5(a), for sufficiently large $w > w_0 = 2z - 1$, $D_{\bar{V}} = 2z - 1$. This scaling is also retrieved for other types of short-range interactions (e.g., finite range or exponentially suppressed), as we show in detail in Appendix E. Since $z > 1$ at the critical point, interactions are always irrelevant in this case. This justifies the findings of previous sections near $U = U_2 = 0$. For $w < w_0$, the finite-size results shown in Fig. 5(b) are compatible with $D_{\bar{V}} = w$. In this case, interactions become relevant for $w < z$ since at that point we start having $D_{\bar{V}} < z$ and thus $D_U > 0$. The nature of this interesting fixed point is left for future exploration.

VIII. DISCUSSION

For a broad class of quasiperiodic models, we provided solid evidence that (i) short-range interactions are irrelevant at the LL-AG transition, not affecting the noninteracting critical exponents; (ii) a many-body generalization of the theory proposed in Ref. [52] can be formulated; and (iii) in the limit of vanishing interactions, the noninteracting critical point is robust to any short-range (and even some long-range) interactions. Our work not only provides a unified understanding of quasiperiodic-induced LL-AG transitions around criticality in terms of flows to noninteracting fixed-points accompanied by the emergence of many-body dualities in widely different models, but it also offers a very precise way to estimate the critical points. Our results contrast with the case of one-dimensional particles experiencing regular Anderson disorder. Differently from the quasiperiodic modulation, disorder is relevant even in the absence of interactions, sending the system to an Anderson localized/glass phase [75,76]. For sufficiently attractive interactions, however, a Luttinger liquid phase survives at small disorder [76–80]. The delocalization-localization transition between these phases occurs when the Luttinger parameter takes the value of $K = 3/2$. For the model in Eq. (1), it takes place at $U = -t$ when only $t, U \neq 0$. This is a Berezinskii-Kosterlitz-Thouless transition, in contrast with the interacting quasiperiodic-induced localization transitions studied here, which we found to be of second-order, as in the noninteracting case. For bosons, there are also well-known both disorder-induced [76,81–84] and quasiperiodic-induced [7,38,85–88] transitions into Bose glass localized phases. It would also be interesting to understand whether in this case, where there is no longer a Fermi surface, an extension hidden dualities also emerge around such transitions.

A future interesting question to address is the effect of interactions on critical phases of noninteracting quasiperiodic models, which can arise in generalized Aubry-André models [32,35,89] and in Fibonacci chains [90,91]. In fact, it was recently shown that interactions can become relevant in the critical phase of a generalized Aubry-André model [92]. Further interesting questions include the nature of the fixed point at which long-range interactions become relevant, and the relevance of interactions in the presence of pairing, where superconductivity was recently found to be enhanced in multifractal critical points and phases of spinful quasiperiodic models [93–95], as in disordered critical points [96–98]. In fact, for the Kitaev chain with random nearest-neighbor hoppings, interactions between Majorana fermions were found to be relevant at the noninteracting critical point [99], even though interactions are irrelevant at the critical point of the analogous spinless fermionic model [99–101]. Fundamental differences of this type may be also present in the quasiperiodic case. Finally, it would also be interesting to see in the future how/if the methodologies introduced here can be generalized to higher dimensions and to excited states, quantum dynamics, and Floquet systems, where for the latter hidden dualities were also recently found to exist at the noninteracting level [102].

ACKNOWLEDGMENTS

The authors M.G. and P.R. acknowledge partial support from Fundação para a Ciência e Tecnologia (FCT-Portugal) through Grant No. UID/CTM/04540/2019. B.A. and E.V.C. acknowledge partial support from FCT-Portugal

through Grant No. UIDB/04650/2020. M.G. acknowledges further support from FCT-Portugal through the Grant No. SFRH/BD/145152/2019. B.A. acknowledges further support from FCT-Portugal through Grant No. CEECIND/02936/2017. J.H.P. is patially supported by the Air Force Office of Scientific Research under Grant No. FA9550-20-1-0136, and the Alfred P. Sloan Foundation through a Sloan Research Fellowship. We finally acknowledge the Tianhe-2JK cluster at the Beijing Computational Science Research Center (CSRC), the Bob|Macc supercomputer through computational project Project No. CPCA/A1/470243/2021, and the OBLIVION supercomputer, through projects HPCUE/A1/468700/2021, 2022.15834.CPCA.A1, and 2022.15910.CPCA.A1 (based at the High Performance Computing Center - University of Évora) funded by the ENGAGE SKA Research Infrastructure (Reference No. POCI-01-0145-FEDER-022217 - COMPETE 2020 and the Foundation for Science and Technology, Portugal) and by the BigData@UE project (Reference No. ALT20-03-0246-FEDER-000033 - FEDER and the Alentejo 2020 Regional Operational Program. Computer assistance was provided by CSRC's, Bob-Macc's, and OBLIVION's support teams.

APPENDIX A: SYSTEM SIZE APPROXIMANTS USED IN FINITE-SIZE SIMULATIONS

In our finite-size simulations, we use rational approximants of τ, $\tau_c = p/N$, with p and N coprime numbers. These approximants were chosen to be exact convergents of the continued fraction expansion of τ. This can be done as long as the unit cell defined by τ_c is equal to or larger than the system size, which guarantees that the system remains incommensurate. For our choice, the size of the unit cell is exactly the system size N. We chose the series of approximants given in Table I.

APPENDIX B: ADDITIONAL SCALING COLLAPSES: EXTRACTING ν AND GOING AWAY FROM HALF-FILLING

We start by extracting the critical exponent ν from the raw data on $\delta E_{\kappa\varphi}$, to validate our choice of $\nu = 1$ in the main text. Assuming the ansatz $\delta E_{\kappa\varphi} \propto e^{-N/\xi}$ and that $\xi = g v^{-\nu}(N, \boldsymbol{\lambda})$, we have $\Lambda_{\kappa\varphi} = \ln\delta E_{\kappa\varphi} = -N v^{\nu}(N, \boldsymbol{\lambda})/g$ (note that $\delta E_{\kappa\varphi} = 1$ for $v = 0$) and therefore, we have $\ln|\Lambda_{\kappa\varphi}| = \ln N + \nu \ln v - \ln g$. We therefore carry out a linear multivariate fit using the data points $(\ln N, \ln|v|, \ln|\Lambda_{\kappa\varphi}|)$ to extract ν and $\ln g$. The results are in Fig. 6, where we show the fitting results as a function of the range $|\Delta v|$ below which data points were selected. The final results $\nu = 1.001 \pm 0.007$ and $g = 0.972 \pm 0.033$ were obtained by averaging the results (and fitting errors) for ν and g, for all the considered windows Δv.

For the noninteracting Aubry-André model, we have that $|\xi| = |1/\ln(2t/V)|$ and therefore for $v \to 0$ we have $|\xi| = |v|^{-1}$ and $|\ln\delta E_{\kappa\varphi}| = -N|v|$. This is consistent with the fitting results obtained for ν and g, which implies that close enough to the critical point, the correlation length behaves in the same way, irrespective of the considered model. Note that in principle, g could depend on $\boldsymbol{\lambda}$ (the remaining parameters of the model), but we observed here for the studied models that close enough to criticality, $g \approx 1$.

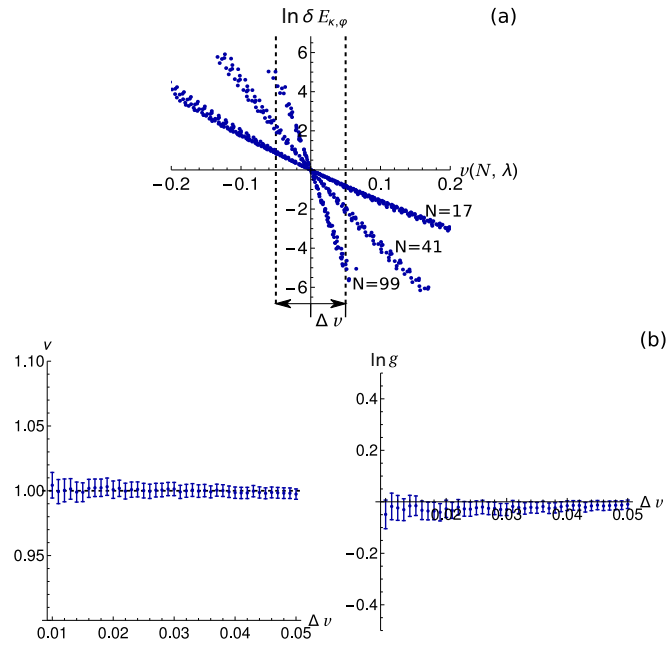

FIG. 6. (a) Raw data used for fits to extract ν. Each cluster of points corresponds to a different system size, indicated close to it. (b) Parameters extracted from a linear multivariate fit to the model $\ln|\Lambda_{\kappa\varphi}| = \ln N + \nu \ln|v| - \ln g$, by using data points $(\ln N, \ln v, \ln|\Lambda_{\kappa\varphi}|)$ selected for different windows Δv [represented in (a)].

We finally show that the data collapse here observed is not a special feature of half-filling. For that purpose, we also obtain results for a filling $\rho = 1/3$, again using models 1 and 2 defined in the main text. The results are in Fig. 7, showing nice collapses around criticality.

APPENDIX C: ADDITIONAL RESULTS FOR OPEN BOUNDARY CONDITIONS

1. Structure factor

We have seen in the main text that the Luttinger parameter K approaches 1 in the Luttinger liquid phase close to criticality, which implies that the small-q behavior of the static structure factor $S(q)$ is that of a noninteracting system. Here we explore in more detail the $S(q)$ behavior at the critical point and in the localized phase. We will do so in the noninteracting (using the single-particle Hamiltonian) and interacting (using DMRG) cases. Let us derive an expression for $S(q)$ in the former case, using the single-particle eigenstates. In the noninteracting case, one can easily show that

$$S(q) = \frac{1}{N}\sum_{i,j=1}^{N}[(\Phi\Phi^{\dagger})_{ii}\delta_{ij} - (|\Phi\Phi^{\dagger}|^2)_{ij}]e^{iq(i-j)}, \qquad \text{(C1)}$$

where Φ is a matrix containing the occupied single-particle eigenstates in its columns and $|.|^2$ squares all entries of matrix $\Phi\Phi^{\dagger}$.

In Fig. 8 we present results for the noninteracting Aubry-André model. We see that at small q, (i) $2\pi S(q) = Kq$ and

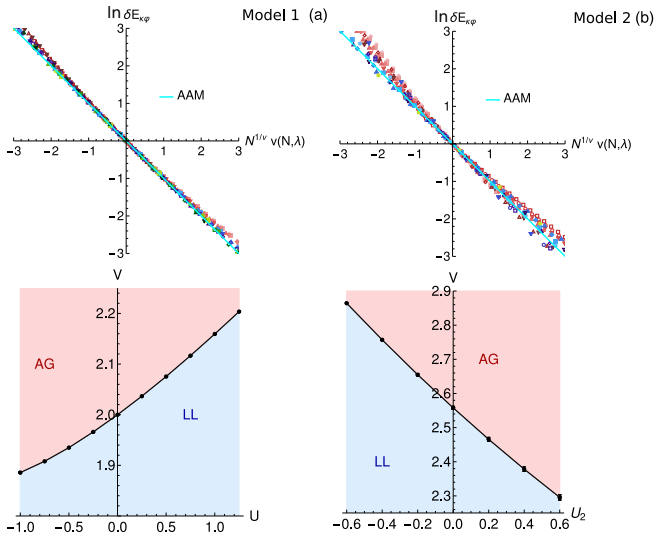

FIG. 7. Results at filling $\rho = 1/3$ for (a) model 1 and (b) model 2 defined in the main text. The bottom panels contain the phase transition points that we take to be $V_c(N = 99, \boldsymbol{\lambda})$ (where $\boldsymbol{\lambda}$ contains the model parameters) with an error computed through $|V_c(99, \boldsymbol{\lambda}) - V_c(41, \boldsymbol{\lambda})|$ (the difference in estimates for the largest used system sizes). Since the error is very small, $V_c(N = 99, \boldsymbol{\lambda})$ already provides a very accurate estimation of $V_c(N = \infty, \boldsymbol{\lambda})$.

$K \approx 1$ in the extended phase; (ii) $2\pi S(q) = Kq(1 + a\sin[b + c\ln(q)])$ and $K \approx 0.7$ at the critical point; (iii) $S(q) \sim q^2$ in the localized phase. Interestingly, at the critical point, there are clear $\ln(q)$-periodic oscillations.

We now consider the family of interacting models given by Eq. (1) in the main text. The results for different choices of these interacting models are given in Figs. 9 and 10. In Fig. 9, we can see that in the LL phase we still have $S(q) \sim q$. However, we have that $2\pi S(q) = Kq$, with $K \neq 1$ sufficiently away from the critical point since the system becomes a truly interacting LL, as in the $V = 0$ limit. This was illustrated in the main text for repulsive interactions in Fig. 3(b), and we here illustrate for attractive interactions in Fig. 10(a). As the critical point is approached, we have $K \to 1$. Exactly at the critical point, on the other hand, $S(q)$ shows an identical behaviour as in the non-interacting Aubry-Andr model's critical point, see Fig. 10(b). It is remarkable to see that even though there are significant differences for larger q for the different considered (interacting and non-interacting) critical points, the small-q behaviour is the same. Interestingly, the amplitude of the log-periodic oscillations decreases in the interacting critical points, as can be seen in Fig. 10(c). Finally, in the AG phase we have $S(q) \sim q^\eta$ with $\eta \to 2$, compatible with the behaviour in the non-interacting localized phase, as shown in Figs. 9.

2. Natural orbitals

In the main text we have shown that the highest occupied natural orbitals are extended and localized, respectively, at the LL and AG phases, and critical at the critical point. Here we show explicit plots, comparing the results with the density fluctuations $\delta n_i \equiv C_e^{ii}$. The results are in Fig. 11. We can see that when the critical point is approached from the LL phase, δn_i becomes very close to $|\psi_i^{(0)}|^2$, signaling the irrelevance of interactions (in the noninteracting case, these quantities are equal).

To finish this section and complement multifractal analysis carried out in Fig. 3(b) of the main text, we show explicit data for $\langle \mathrm{IPR}_{N0}(q = 2)\rangle_\phi$ as a function of system size N, from which the exponent $\tau(q = 2)$ was extracted. The results are shown in Fig. 12.

3. Entanglement entropy

In the main text, we mentioned that the entanglement entropy, $\mathcal{S}$, shows log-periodic oscillations as a function of the subsystem size, at the critical point of the noninteracting Aubry-André model. In Fig. 13(a) we show the numerical results supporting this claim in a log-linear plot. By averaging $\mathcal{S}$ over a sufficiently large number of ϕ configurations, we see that these oscillations are robust to increasing the system size. In Fig. 13(b) we also show that these oscillations persist in the presence of interactions, at the critical point.

APPENDIX D: DUALITY TRANSFORMATION

Here we build a many-body generalization of the duality transformation introduced in Ref. [48]. We start by writing the most occupied natural orbital as $|\alpha = 0\rangle = \sum_i \psi_i^{(0)} |i\rangle$, and defining its Fourier transform as

$$\tilde{\psi}_k^{(0),d} = \frac{1}{\sqrt{N}} \sum_{i=0}^{N-1} e^{i2\pi\tau_c ki} \psi_i^{(0)}. \tag{D1}$$

The hidden duality transformations defined in Ref. [48] map points $(\phi, k) = (\phi_0 + \Delta\phi, k_0 + \Delta k)$ to points $(\phi', k') = (\phi_0 + \Delta k, k_0 + \Delta\phi)$, where (ϕ_0, k_0) is the center of the hidden duality transformation. Setting $(\phi_0, k_0) = (\varphi_0, \kappa_0)$, with (φ_0, κ_0) given in the main text for the different used system sizes yields a possible choice for which $\boldsymbol{\psi}^{(0)} \propto \tilde{\boldsymbol{\psi}}^{(0),d}$ at the self-dual point of the noninteracting Aubry-André model ($V = 2$). For more generic choices, we would need to compute $\psi_i^{(0)}$ at $(\phi, k) = (\phi_0 + \Delta\phi, k_0 + \Delta k)$ and $\tilde{\psi}_k^{(0),d}$ at $(\phi', k') = (\phi_0 + \Delta k, k_0 + \Delta\phi)$ to have $\boldsymbol{\psi}^{(0)} \propto \tilde{\boldsymbol{\psi}}^{(0),d}$.

In Fig. 14(a) we computed $F_{RK} \equiv (\tilde{\boldsymbol{\psi}}^{(0),d})^* \cdot \boldsymbol{\psi}^{(0)}$ using $(\phi, k) = (\phi_0, k_0) = (\varphi_0, \kappa_0)$ for model 1 with $U = 0.5$ as an example. We see that F_{RK} decreases with N, except when we cross the critical point, where it becomes very close to 1. This suggests that $\boldsymbol{\psi}^{(0)}$ is almost equal to $\tilde{\boldsymbol{\psi}}^{(0),d}$ at this point. We can go one step further and define the duality transformation that relates $\boldsymbol{\psi}^{(0)}$ and $\tilde{\boldsymbol{\psi}}^{(0),d}$ at self-dual points as in Ref. [48] (where the natural orbital replaces the role of the single-particle wave function).

From $\boldsymbol{\psi}^{(0)}$ and $\tilde{\boldsymbol{\psi}}^{(0),d}$, we then define the duality matrix $\mathcal{O}_c$ as in Ref. [48]:

$$\mathcal{O}_c[T^n \tilde{\boldsymbol{\psi}}^{(0),d}] = T^n \boldsymbol{\psi}_i^{(0)}, \quad n = 0, \cdots, L-1, \tag{D2}$$

where T is the cyclic translation operator defined as $T\psi = \psi'$ with $\psi_i' = \psi_{\ \mathrm{mod}\ (i+1,L)}$. Since $\mathcal{O}_c$ is a circulant matrix, we may write it as

$$\mathcal{O}_c = U^\dagger W U, \tag{D3}$$

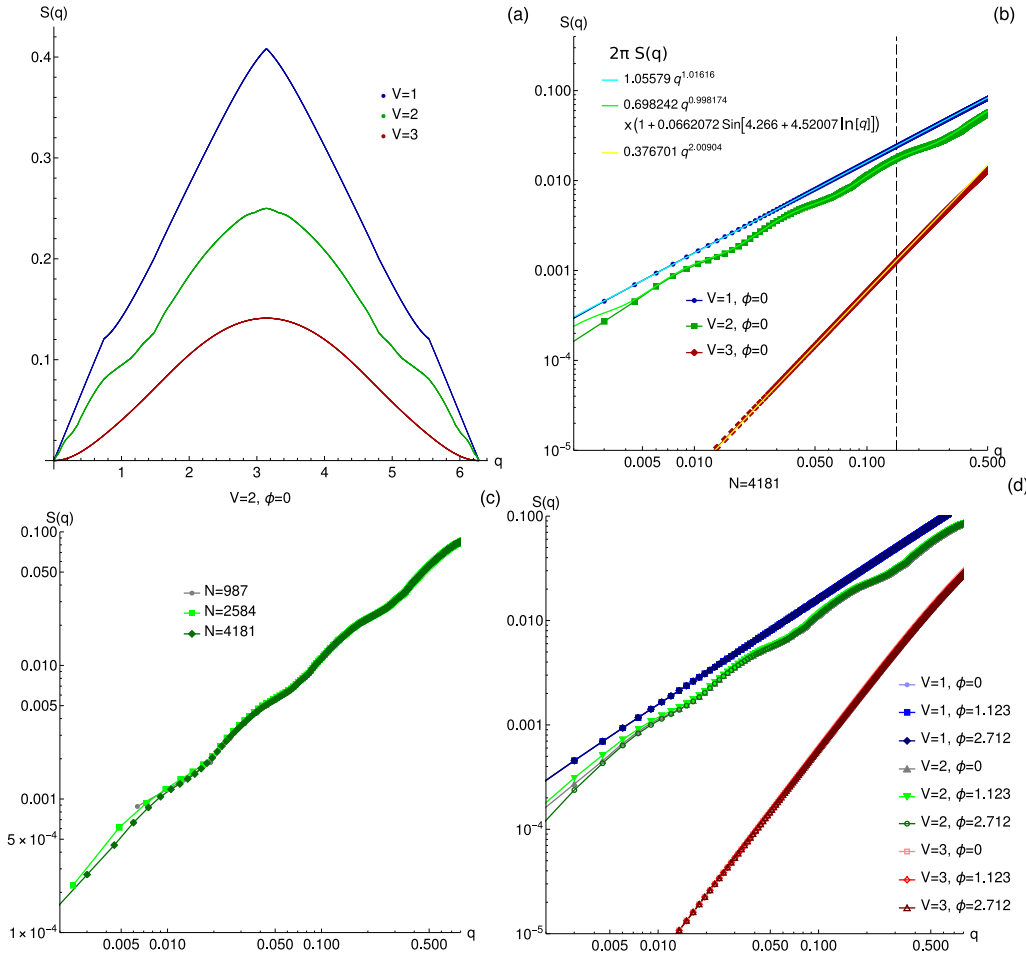

FIG. 8. Results for noninteracting Aubry-André model, at half-filling [$N_p = \lfloor \rho N \rfloor$, where $\lfloor x \rfloor$ takes the integer part of x and $\rho = 1/2$], using open boundary conditions. (a) Results for $V = 1$ (extended phase), $V = 2$ (critical point), and $V = 3$ (localized phase). (b) Low-q behavior of $S(q)$. The vertical dashed line denotes the largest q considered for the fits to the expressions: (i) $2\pi S(q) = Kq^{\eta}$ in the extended phase, where we obtained K, $\eta \approx 1$; (ii) $2\pi S(q) = Kq^{\eta}(1 + a\sin[b + c\ln(q)])$ in the critical phase, where we extracted $K \approx 0.7$ and $\eta \approx 1$; (iii) $S(q) \sim q^{\eta}$ in the localized phase, where we extracted $\eta \approx 2$. Note that at the critical point, there are clear log-periodic oscillations. These are not a finite-size effect, as can be seen in (c), where different system sizes were considered and the oscillations are robust. (d) Dependence of $S(q)$ on ϕ, for fixed $N = 4181$. The results for different choices or ϕ are essentially the same, except at the critical point for small q, where there is a slight ϕ dependence, for fixed N.

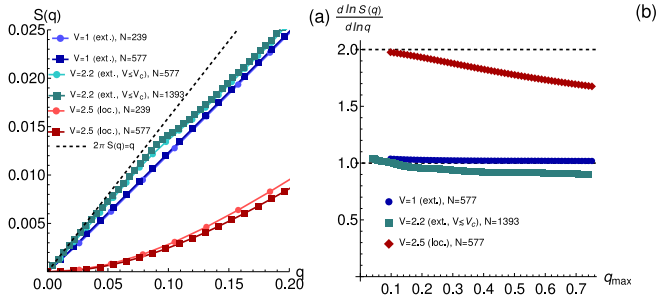

FIG. 9. Results for interacting models, at half-filling, using open boundary conditions. (a) $S(q)$ for $U = 1$ and $U_2 = t_2 = V_2 = 0$, $\phi = 1.123$, for V in the LL/extended phase ($V = 1$), in the LL phase but close to the critical point ($V = 2.2$), and in the AG phase ($V = 2.5$). (b) Assuming that $S(q) \sim q^{\eta}$, we extract $\eta \equiv \partial \ln S(q)/\partial \ln q$ by making a linear fit to the $\ln S(q)$ vs. $\ln q$ data, from $q = 0$ up to $q = q_{\max}$ (given in the x axis of the figure). We see that in the LL phase, $\eta \approx 1$, while in the AG, $\eta \to 2$, as in the noninteracting case.

where U is a matrix with entries $U_{ij} = e^{2\pi i \tau_c ij}$ and W is a diagonal matrix $W_{ij} = w_j \delta_{ij}$ with the eigenvalues $\{w_j\}$ of $\mathcal{O}_c$. We can therefore write

$$\boldsymbol{\psi}^{(0)} = U^{\dagger} W \boldsymbol{\psi}^{(0)} \leftrightarrow \psi_i^{(0)} = \sum_{\nu=0}^{L-1} e^{2\pi i \tau_c ij} w_j \psi_j^{(0)}. \tag{D4}$$

The eigenvalues w_j are, as seen in Ref. [48], evaluations of a function $W(x)$, that has period $\Delta x = 1$, at points $x_j = \mathrm{mod}\,(j\tau_c + \frac{\phi}{2\pi}, 1)$, $j = 0, \ldots, L-1$. This function is sampled in the whole interval $x \in [0, 1[$ in the limit that $\tau_c \to \tau$ ($N \to \infty$) and encodes all the information on the duality transformation W. We show an example of the duality function $W(x)$ in Fig. 14(b), where we see that a complicated function with features that are robust to the increasing of N is formed. $W(x_j)$ only has the meaning of a duality transformation if $\boldsymbol{\psi}^{(0)}$ and $\tilde{\boldsymbol{\psi}}^{(0),d}$ are computed at self-dual points (or at dual points in the extended and localized phases, a case that

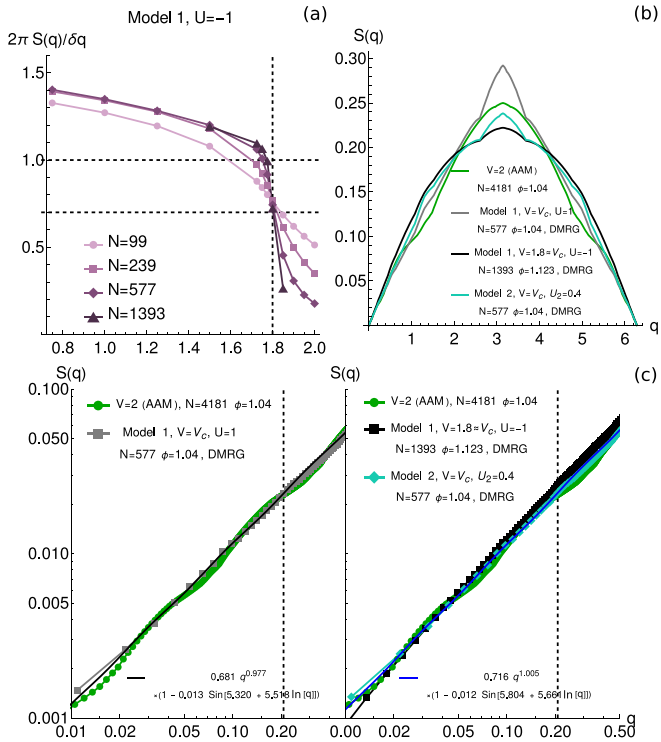

FIG. 10. Results for interacting models, at half-filling, using open boundary conditions. (a) Slope of structure factor $S(\delta q)$ as a function of V for model 1 with attractive interaction $U = -1$, and $\phi = 1.123$. (b) $S(q)$ at critical points obtained with significantly different parameters indicated in the figure, including the noninteracting case. We can see that in all cases, the small q behavior is very similar. (c) Log-log plot for the data in (b), along with fits to the expression $2\pi S(q) = Kq^{\eta}(1 + a\sin[b + c\ln(q)])$ for the interacting critical points, with the fit parameters given in the figure. Note that the vertical dashed line in the right panel denotes the largest q considered for the fits. Neglecting the log-periodic oscillations, we get $2\pi S(q) = Kq$, with $K \approx 0.7$ in all cases.

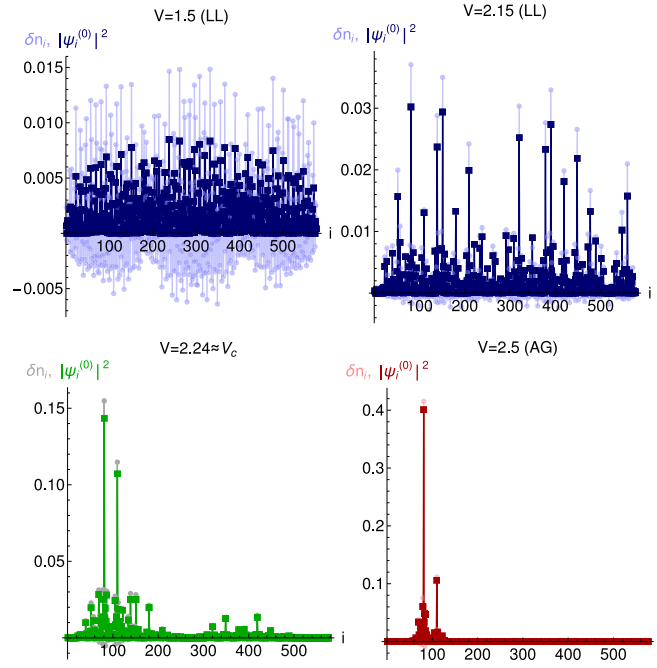

FIG. 11. Plots of the squared amplitudes of natural orbitals, $|\psi_i^{(0)}|^2$, and of the density fluctuations δn_i for $N = 577$, with $U = 1$ and $U_2 = t_2 = V_2 = 0$, and $\phi = 1.123$, for different V.

was not considered here). We can, however, compute $W(x_j)$ in the same way by using $\boldsymbol{\psi}^{(0)}$ and $\tilde{\boldsymbol{\psi}}^{(0),d}$ at any point, but in this case, since there is no duality transformation connecting the wave functions, we expect $W(x_j)$ to be featureless and not robust for increasing system size. This is clearly shown in the insets of Fig. 14(b).

APPENDIX E: GENERALIZED CHALKER SCALING AND IRRELEVANCE OF GENERIC SHORT-RANGE INTERACTIONS

We show that generic short-range (and some long-range) interactions are irrelevant at the critical point of the Aubry-André model in the $U \to 0$ limit, by unveiling the existence of a generalized Chalker scaling [70–74] at this point. All the results that we present in this section are for the parameters studied in the main text, namely $\tau = 1/\sqrt{2}$ and at half-filling, with $N_p = \lfloor N/2 \rfloor$ particles. Nonetheless, the technology here developed can be (and was) applied to more generic cases, as we comment at the end of the section.

We consider the periodized form of the power-law interactions $U \sum_j j^{-w} n_r n_{r+j}$, given by

$$U \sum_{j=1}^{N-1} \sum_{k=0}^{\infty} (j + kN)^{-w} \sum_r n_r n_{r+j+kN} \tag{E1}$$

$$= U \sum_{j=1}^{N-1} N^{-w} \zeta(w, j/N) \sum_{r=1}^{N} n_r n_{r+j}, \tag{E2}$$

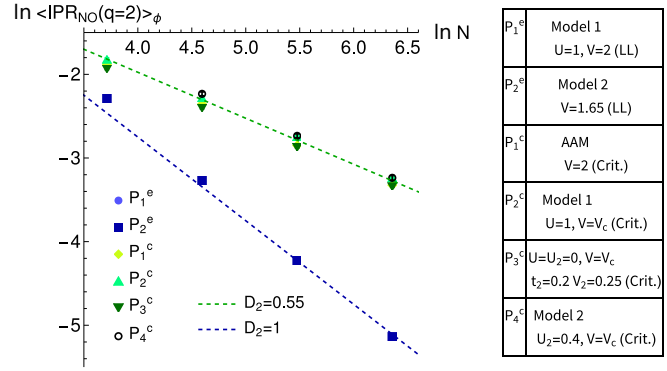

FIG. 12. $\langle \mathrm{IPR}_{N0}(q = 2)\rangle_\phi$ for different models with chosen parameters indicated in the table at right, where P_i^e (P_i^c) denote extended (critical) points. In the table, V_c corresponds to the estimated critical point. $\langle\rangle_\phi$ denotes an average over different choices of ϕ. We took $\phi_j = 2\pi j/N_c$, $j = 0, \cdots, N_c - 1$, and $N_c \in [100\text{–}300]$. The blue and green dashed lines in (c) shows the scaling behavior in the noninteracting Aubry-André model, respectively at extended and critical points.

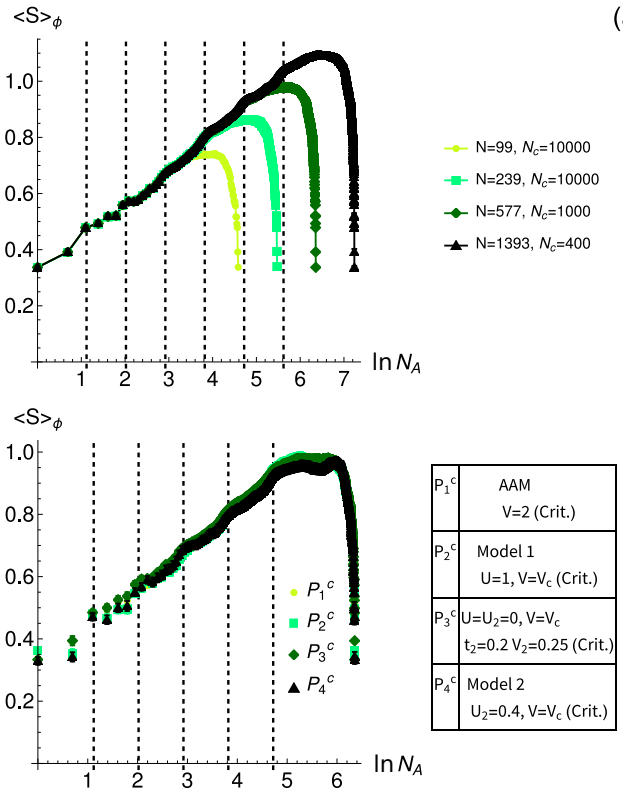

FIG. 13. (a) Entanglement entropy $\mathcal{S}$ as a function of the size of subsystem A, consisting of the first N_A sites, for the noninteracting Aubry-André model. We used different system sizes and averaged over N_c configurations of ϕ given by $\phi_j = 2\pi j/N_c$, , $j = 0, \ldots, N_c - 1$. The vertical dashed lines are guides to the eye, showing the log-periodic maxima of the oscillations. (b) DMRG results at different critical points obtained for the parameter choices given in the table, averaging over $N_c \in [100\text{–}300]$ configurations.

where $\zeta(w, y) = \sum_{k=0}^{\infty}(k + y)^{-w}$ is the Hurwitz zeta function and $c_r^\dagger = c_{r+kN}^\dagger, k \in \mathbb{Z}$ due to periodic boundary conditions. For such interaction, we can write the path integral for the Grassman variables $\bar{c}, c$ as

$$Z = \int \mathcal{D}[\bar{c}, c] e^{-(S_0[\bar{c},c]+S_U[\bar{c},c])}, \tag{E3}$$

where, writing in the single-particle eigenbasis of the noninteracting Aubry-André model Hamiltonian H_0 [Eq. (1) of the main text, with $t_2 = V_2 = U = U_2 = 0$] with eigenenergies $\epsilon_\alpha = E_\alpha - \mu$ (measured relative to the chemical potential μ), we have

$$S_0 = \int_0^\infty d\tau \sum_\alpha \bar{c}_\alpha(\tau)(\partial_\tau + \epsilon_\alpha)c_\alpha(\tau) \tag{E4}$$

$$S_U = -U \int_0^\infty d\tau \sum_{\alpha,\beta,\gamma,\delta} \bar{V}_{\alpha\beta\gamma\delta}\bar{c}_\alpha(\tau)\bar{c}_\beta(\tau)c_\gamma(\tau)c_\delta(\tau) \tag{E5}$$

and where $\bar{V}_{\alpha\beta\gamma\delta} = (V_{\alpha\beta\gamma\delta} - V_{\beta\alpha\gamma\delta} + V_{\beta\alpha\delta\gamma} - V_{\alpha\beta\delta\gamma})/4$ is the antisymmetrized version of the interaction matrix elements

$$V_{\alpha\beta\gamma\delta} = \sum_{r=1}^{N}\sum_{j=1}^{N-1} N^{-w}\zeta(w, j/N)\,\langle\alpha|r\rangle \times \langle\beta|r + j\rangle\,\langle r|\gamma\rangle\,\langle r + j|\delta\rangle\,. \tag{E6}$$

We will now inspect the interacting part in detail. We have a four-leg tensor on our hands. We want to study this tensor close to $\alpha, \beta, \gamma, \delta = 0$, where 0 denotes the Fermi level. Since the tensor is antisymmetric, $\bar{V}_{0000} = 0$. We can now inspect different combinations of indices to see how the four-leg tensor behaves as the indices depart from 0. We can start by fixing three of the indices to be 0 and varying the remaining index. However, this yields zero due to antisymmetry. We can also now fix two indices to 0 and vary the remaining two indices that we call α and β. The possible contributions are $\bar{V}_{0\alpha0\beta}$, $\bar{V}_{\alpha0\beta0} = \bar{V}_{0\alpha0\beta}$, $\bar{V}_{00\alpha\beta} = \bar{V}_{\alpha\beta00} = 0$, and $\bar{V}_{\alpha00\beta} = \bar{V}_{0\alpha\beta0} = -\bar{V}_{0\alpha0\beta}$. Therefore, the only contribution that we need to compute is $\bar{V}_{0\alpha0\beta}$, as all the others are either zero or can be obtained from this one. In Fig. 15 we show that the most important contribution arises for $\alpha = \beta$ (we show examples for $w = 1.5$ and $w = 3$, but this remains true for other values of w). Therefore, we will focus on the contribution $\bar{V}_{0\alpha0\alpha}$. Note that higher-order contributions involve setting only one index to 0 and varying the others, but is already a contribution involving three energies, which we assume to be negligible as $\alpha, \beta, \gamma, \delta \to 0$. We then write the interacting part of the action as

$$S_U = -4U \int_0^\infty d\tau \sum_\alpha \bar{V}_{0\alpha0\alpha}\bar{c}_0(\tau)\bar{c}_\alpha(\tau)c_0(\tau)c_\alpha(\tau) + \mathcal{O}(\epsilon_\alpha^\mu \epsilon_\gamma^x), \tag{E7}$$

where we assumed that $\bar{V}_{0\alpha0\alpha} \sim \epsilon_\alpha^\mu$ and γ denotes the additional index (or indices) that we choose to make finite in tensor $\bar{V}_{0\alpha0\alpha}$ [for instance $\bar{V}_{0\alpha\gamma\alpha} = \bar{V}_{0\alpha0\alpha} + \mathcal{O}(\epsilon_\alpha^\mu \epsilon_\gamma^x)$] and the exponent x may depend on this choice of indices. This contribution will therefore either be negligible or the same as of $\bar{V}_{0\alpha0\alpha}$, if $x = 0$. The term $\bar{V}_{0\alpha0\alpha}$ can be written explicitly as

$$\bar{V}_{0\alpha0\alpha} = \frac{1}{4}\sum_{j=1}^{N-1} N^{-w}\zeta(q, j/N)\left(\sum_{r=1}^{N}(|\langle 0|r\rangle|^2|\langle\alpha|r + j\rangle|^2 + |\langle\alpha|r\rangle|^2|\langle 0|r + j\rangle|^2) - \sum_{r=1}^{N}\langle 0|r\rangle\langle r|\alpha\rangle\langle\alpha|r + j\rangle\langle r + j|0\rangle - \sum_{r=1}^{N}\langle\alpha|r\rangle\langle r|0\rangle\langle 0|r + j\rangle\langle r + j|\alpha\rangle\right). \tag{E8}$$

In Figs. 16(a), 16(b) we show that it is possible to collapse the results for $\bar{V}_{0\alpha0\alpha}$ for different approximant system sizes and different energies. The collapse becomes better as $\epsilon_\alpha \to 0$. Furthermore, there are clusters of eigenvalues that form on

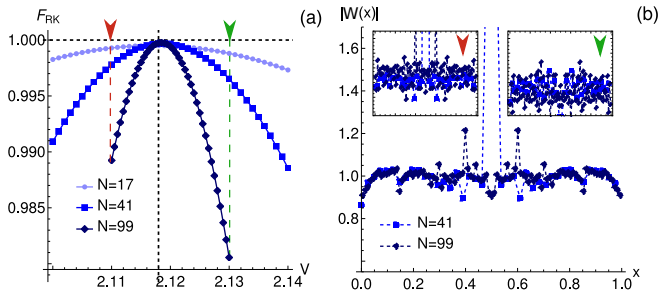

FIG. 14. (a) F_{RK} defined in the text for $U = 0.5$ and $U_2 = V_2 = t_2 = 0$. The dashed black line indicates $V = V_c(N = 99)$. (b) Duality function $\chi(x)$ introduced in Ref. [48] defined through the natural orbital at $V = V_c(N)$. The insets show the results if $\chi(x)$ was computed at the points marked in (a), slightly away from the critical point: in this case we obtain a featureless function, not robust to increasing N. We use exactly the same scale in the insets that we use in the main figure.

the $\ln|\epsilon_\alpha|$ scale, that we will call minibands in the following. In Fig. 16(c) we can see that the number of states in each miniband scales as $N_{\mathrm{mb}(n)} \propto p^n$. By realizing that increasing the order of system size approximant introduces a new miniband, we can easily find that $p = N_{m+1}/N_m \to 1 + \sqrt{2}$ as $m \to \infty$ where N_m is the mth order system size approximant for $\tau = 1/\sqrt{2}$. By defining $\bar{\epsilon}_n^{(m)} = N_{\mathrm{mb}(n)}^{-1} \sum_{\alpha \in \mathrm{mb(n)}} \epsilon_\alpha^{(m)}$ [where the superscript (m) indicates the eigenenergies for the m-th order size approximant], we also have that $\bar{\epsilon}_n \propto p^{nz}$, as indicated in Fig. 16(a), where $z = 1.575$ is the dynamical critical exponent. Naturally, the scaling collapse in this figure also implies that $\epsilon_\alpha^{(m-l)} = p^{zl}\epsilon_\alpha^{(m)}$. These observations allow us to write the following ansatz,

$$\bar{V}_{0\alpha 0\alpha} = \mathcal{C} N_m^{-D_{\bar{V}}} (|\epsilon_\alpha^{(m)}| N_m^z)^\mu \sum_n f_n([|\epsilon_\alpha^{(m)}| - \bar{\epsilon}_n^{(m)}] N_m^z), \quad \text{(E9)}$$

where $\mathcal{C}$ is some constant independent of energy and N_m, and f_n are scaling functions. We note that, as shown in Figs. 16(a), 16(b) and in the main text, $D_{\bar{V}}$ depends on w. We will discuss this dependence in more detail below. At this point we also note that when averaged over minibands, $\bar{V}_{0\alpha 0\alpha} \sim (|\epsilon_\alpha^{(m)}|)^\mu$, where $\mu > 0$. This shows that there is a generalized Chalker scaling [70–74] at the critical point of the Aubry-André model, manifested by power-law correlations (on average) between the single-particle eigenfunctions with respect to their energy difference.

To carry out a power-counting analysis and inspect the scaling dimension of the interactions, we take a large enough system size to begin with so that the data collapse is quite good for the relevant energies of choice and Eq. (E9) holds. In each renormalization-group (RG) step, we throw away a miniband and rescale the energies. Starting with an energy cutoff Λ_k,

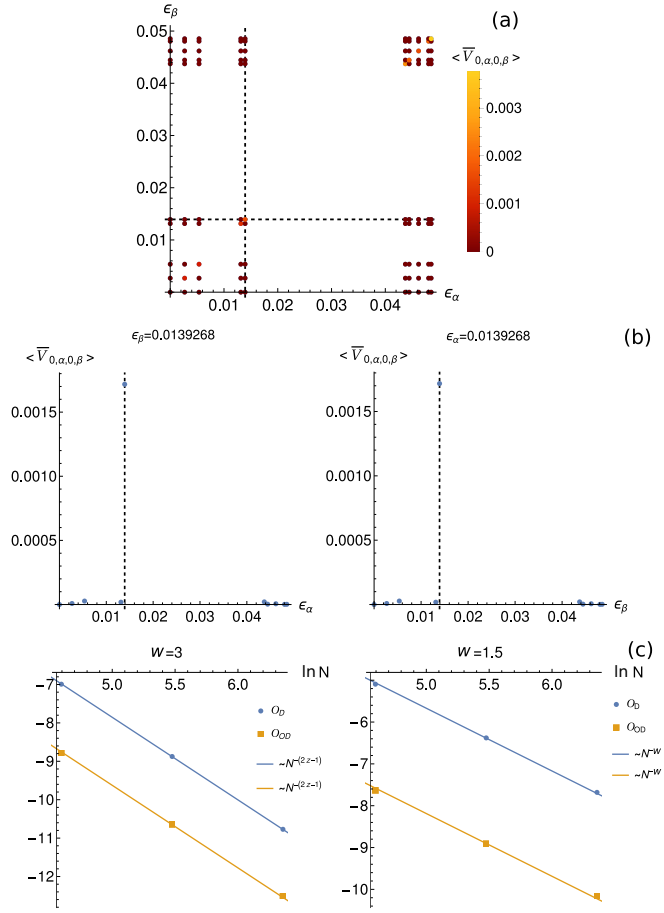

FIG. 15. (a) $\langle \bar{V}_{0\alpha 0\beta} \rangle_{\phi,\kappa}$ for $N = 239$, $w = 1.5$, and $\alpha, \beta = 0, \ldots, 9$, averaged over 200 random configurations of ϕ and κ. We can see that the dominant contribution occurs for $\alpha = \beta$. This can also be seen in (b), where we make the cuts marked in (a) by the dashed lines. The vertical dashed line in (b) indicates the diagonal contribution, which is much larger than the remaining ones. In (c) we show that this conclusion is robust to increasing N. To do so, we compute the average diagonal, $\mathcal{O}_{\mathrm{OD}} = \frac{1}{n^2-n} \sum_{\alpha \neq \beta}^{n} \langle \bar{V}_{0\alpha 0\beta} \rangle_{\phi,\kappa}$, and off-diagonal, $\mathcal{O}_{\mathrm{D}} = \frac{1}{n} \sum_{\alpha=1}^{n} \langle \bar{V}_{0\alpha 0\alpha} \rangle_{\phi,\kappa}$, contributions (fixing $n = 9$, independently of N). Results are shown for $w = 3$ (left) and $w = 1.5$ (right) as examples. $\mathcal{O}_{\mathrm{OD}}$ and $\mathcal{O}_{\mathrm{D}}$ scale identically with N, implying that the diagonal contribution dominates for any N.

after l RG steps we end up with a cutoff $\Lambda_{k+l} = \Lambda_k/p^{zl}$. We also start with an initial system size N_m. The noninteracting action S_0, after introducing the cutoff, is given by

$$S_0^{\Lambda_k, N_m} = \int_0^\infty d\tau \int_{-\Lambda_k}^{\Lambda_k} d\epsilon \sum_\alpha \delta\big(\epsilon - \epsilon_\alpha^{(m)}\big)\bar{c} \times (\epsilon, \tau)(\partial_\tau + \epsilon) c(\epsilon, \tau). \quad \text{(E10)}$$

After l RG steps, it becomes:

$$S_0^{\Lambda_{k+l}, N_m} = \int_0^\infty d\tau' \int_{-\Lambda_k}^{\Lambda_k} d\epsilon' \sum_\alpha \delta\big(\epsilon' - \epsilon_\alpha^{(m-l)}\big)\bar{c}(\epsilon', \tau')(\partial_{\tau'} + \epsilon') c(\epsilon', \tau') = S_0^{\Lambda_k, N_{m-l}}, \quad \text{(E11)}$$

where we used $\epsilon' = p^{zl}\epsilon$, $\tau' = \tau\, p^{-zl}$, $\epsilon_\alpha^{(m-l)} = p^{zl}\epsilon_\alpha^{(m)}$ and defined $\bar{c}(\epsilon' p^{-zl}, \tau' p^{zl}) = \bar{c}(\epsilon', \tau')$; $c(\epsilon' p^{-zl}, \tau' p^{zl}) = c(\epsilon', \tau')$. The new action after l RG steps therefore corresponds to the same action, but for a smaller system size N_{m-l}. For the interacting part,

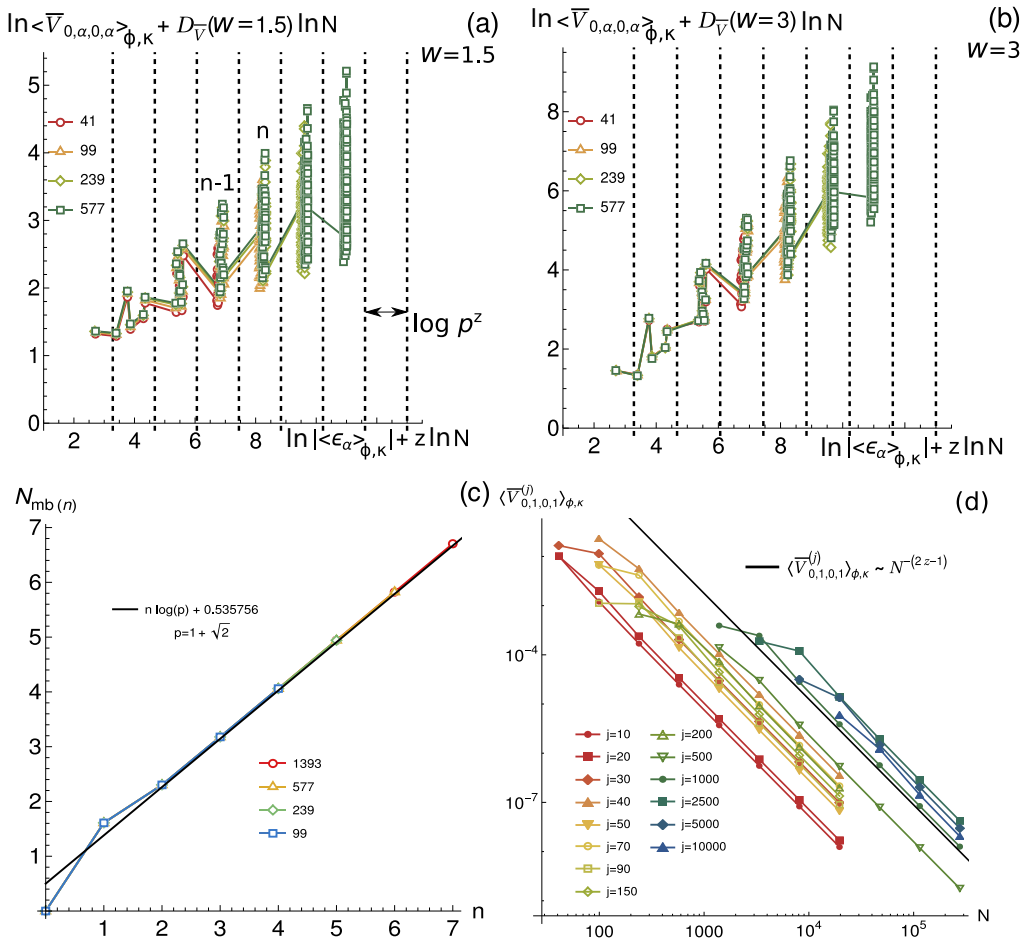

FIG. 16. (a), (b) $\langle \bar{V}_{0\alpha 0\alpha} \rangle_{\phi,\kappa}$ averaged over 200 random configurations of ϕ and κ ($\langle\rangle_{\phi,\kappa}$ denotes the average over ϕ, κ configurations) for (a) $w = 1.5$ and (b) $w = 3$, where $D_{\bar{V}}(w = 1.5) = w$ and $D_{\bar{V}}(w = 3) = 2z - 1$, with $z = 1.575$ being the dynamical critical exponent. (c) Number of states in each miniband, $N_{\mathrm{mb}(n)}$. Note that the minibands are only well-defined (that is, there are clear clusters of states) for $n \geqslant 2$, above which the scaling $N_{\mathrm{mb}(n)} \propto p^n$ is observed. The dashed lines in (a), (b) are separated by $\ln p^z$, implying that the average energy of each miniband scales as p^{zn}. (d) $\langle \bar{V}^{(j)}_{0\alpha 0\alpha} \rangle_{\phi,\kappa}$ for the interaction term in Eq. (E17), and for $\alpha = 1$, as a function of system size N and averaged over 4800 random configurations of ϕ and κ.

we have

$$S_U^{\Lambda_k, N_m} = -UC N_m^{-D_{\bar{V}}} \sum_\alpha \int_{-\Lambda_k}^{\Lambda_k} d\epsilon \delta\big(\epsilon - \epsilon_\alpha^{(m)}\big)(|\epsilon| N_m^z)^\mu \sum_n f\big(\big[|\epsilon| - \bar{\epsilon}_n^{(m)}\big] N_m^z\big) \bar{c}(0,\tau)\bar{c}(\epsilon,\tau)c(0,\tau)c(\epsilon,\tau), \tag{E12}$$

where the factor 4 in Eq. (E7) was absorbed in the constant $\mathcal{C}$. The full action for the interacting part after l RG steps is therefore

$$\begin{aligned} S_U^{\Lambda_{k+l}, N_m} =& -UCp^{-(D_{\bar{V}}-z)l} N_{m-l}^{-(D_{\bar{V}}-z)} \int d\tau' \sum_\alpha \int_{-\Lambda_k}^{\Lambda_k} d\epsilon' \, \delta\big(\epsilon' - \epsilon_\alpha^{(m-l)}\big)\big(|\epsilon'| N_{m-l}^z\big)^\mu \\ & \times \sum_n f\big(\big[|\epsilon'| - \bar{\epsilon}_n^{(m-l)}\big] N_{m-l}^z\big) \bar{c}(0,\tau')\bar{c}(\epsilon',\tau')c(0,\tau')c(\epsilon',\tau') \\ =& \, p^{-(D_{\bar{V}}-z)l} S_U^{\Lambda_k, N_{m-l}}. \end{aligned} \tag{E13}$$

In summary, after l RG steps we have:

$$S^{\Lambda_{k+l}, N_m} = S_0^{\Lambda_{k+l}, N_m} + S_U^{\Lambda_{k+l}, N_m} \tag{E14}$$

$$= S_0^{\Lambda_k, N_{m-l}} + p^{-(D_{\bar{V}}-z)l} S_U^{\Lambda_k, N_{m-l}}. \tag{E15}$$

This implies that the scaling dimension of the interacting part is $D_U = z - D_{\bar{V}}$, and therefore interactions are irrelevant when $D_{\bar{V}} > z$. In Fig. 4(b) of the main text, we have seen that the thermodynamic-limit behavior of $D_{\bar{V}}(w)$ is compatible

with

$$D_{\bar{V}}(w) = \begin{cases} w, & w < 2z-1 \\ 2z-1, & w \geqslant 2z-1 \end{cases}. \tag{E16}$$

This implies that interactions are irrelevant for $w > z$, marginal for $w = z$ and relevant for $w < z$. The relevance of interactions for $w < z$ is left for future exploration. These results also imply that even when long-range interactions are considered, they can be irrelevant in the $U \to 0$ limit if they decay fast enough. On the other hand, it also follows that short-range interactions have $D_{\bar{V}} = 2z - 1$ and therefore their scaling dimension is $D_U = 1 - z$. Since $z > 1$ at the critical point, short-range interactions are irrelevant. At the extended phase, on the other hand, $z = 1$, which implies that interactions are marginal, in agreement with the $V = 0$ results.

To show that short-range interactions are irrelevant in more detail, we consider the following finite-range interacting terms (again assuming periodic boundary conditions),

$$H_U^{(j)} = U \sum_{r=1}^{N} n_r n_{r+j} \tag{E17}$$

and compute the associated antisymmetrized interaction $\bar{V}_{0101}^{(j)} \propto N^{-D_{\bar{V}}}$ for each interaction term of this type, in Fig. 16(d). We find that no matter the interaction range j, if the system size becomes sufficiently larger than this range $D_{\bar{V}}(N) \to 2z - 1$. Therefore, any short-range function of these interaction terms should also follow this behavior. With this in mind, we expect that the universal behavior unveiled in this work is not restricted to the interactions studied in Eq. (1) of the main text, but also holds for more generic short-range (and even some long-range) interactions. Even though in this section we focused on the choices of parameters used in the main text, we checked that the same conclusions can also be drawn for other fillings and other values of τ also considered in Ref. [28].

We finish this section by showing that the short-range dimension $D_{\bar{V}} = 2z - 1$ can be understood from simple arguments. We start by writing

$$\bar{V}_{0101} = N^{-D_{\bar{V}}} h(\epsilon_g N^z) \tag{E18}$$

assuming that $D_{\bar{V}}$ is unknown, where ϵ_g is the energy gap for a system size N, and h is a scaling function. Since we have $\epsilon_g = \Upsilon N^{-z}$, where Υ is a constant, we know that $\bar{V}_{0101} = N^{-D_{\bar{V}}} f(\Upsilon) \sim N^{-D_{\bar{V}}}$ and therefore

$$\bar{V}_{0101} = \epsilon_g^{D_{\bar{V}}/z}. \tag{E19}$$

On the other hand, we can write

$$\bar{V}_{0101} = \sum_{r=1}^{N} \bar{V}_{\epsilon_g}^r, \tag{E20}$$

where

$$\bar{V}_{\epsilon_g}^r = \frac{1}{4}\big(|\langle 0|r\rangle|^2 |\langle 1|r+j\rangle|^2 + |\langle 1|r\rangle|^2 |\langle 0|r+j\rangle|^2 - (\langle 0|r\rangle \langle r|1\rangle \langle 1|r+j\rangle \langle r+j|0\rangle + \text{c.c})\big). \tag{E21}$$

After averaging over ϕ and κ, translational invariance is restored and $\bar{V}_{\epsilon}^r$ becomes r independent. Furthermore, we know that $\bar{V}_{\epsilon_g}^r \to 0$ as $\epsilon_g \to 0$. Expanding $\bar{V}_{\epsilon_g}^r$ in powers of ϵ_g, assuming it to be a regular function:

$$\bar{V}_{\epsilon_g}^r = a_1 \epsilon_g + a_2 \epsilon_g^2 + \cdots. \tag{E22}$$

We have that $a_1 = 0$ since it can be easily shown that $\bar{V}_{\epsilon_g}^r \geqslant 0$ for any ϵ_g. We therefore have

$$\bar{V}_{0101} \sim N \epsilon_g^2 \sim \epsilon_g^{2-1/z}. \tag{E23}$$

By comparing with Eq. (E19), this therefore implies that $D_{\bar{V}} = 2z - 1$. Therefore, we conclude that the scaling dimension for short-range interactions simply follows from $\bar{V}_{\epsilon_g}^r$ being a regular function of ϵ_g.

TABLE II. Choices of sizes N, rational approximants τ_c, and number of ϕ configurations N_c for $\tau = 1/\sqrt{2}$ and $\tau = (\sqrt{5}-1)/2$. The different phases ϕ were chosen from a uniform grid given by $\phi_j = 2\pi j/N_c$, $j = 0, \ldots, N_c - 1$.

$\tau = 1/\sqrt{2}$						
N	41	99	239	577	1393	3363
τ_c	$\frac{29}{41}$	$\frac{70}{99}$	$\frac{169}{239}$	$\frac{408}{577}$	$\frac{985}{1393}$	$\frac{2378}{3363}$
N_c	500	500	500	500	500	300

$\tau = (\sqrt{5}-1)/2$											
N	34	55	89	144	233	377	610	987	1597	2584	4181
τ_c	$\frac{21}{34}$	$\frac{34}{55}$	$\frac{55}{89}$	$\frac{89}{144}$	$\frac{144}{233}$	$\frac{233}{377}$	$\frac{377}{610}$	$\frac{610}{987}$	$\frac{987}{1597}$	$\frac{1597}{2584}$	$\frac{2584}{4181}$
N_c	1000	1000	1000	1000	750	750	500	500	500	300	250

APPENDIX F: CHARGE GAP SCALING FOR ALTERNATIVE CHOICES OF τ AND FILLING ρ

From the results that we obtained in the main text, we have seen that the scalings of the charge gap (and other quantities such as the fractal dimension) with system size obtained at different LL-AG transitions are compatible, no matter the chosen parameters (hoppings, potential, interactions), at half-filling ($\rho = 1/2$) and for approximants of $\tau = 1/\sqrt{2}$ (Fig. 3 of the main text). A natural question that arises is whether this is a special feature of our choice of ρ and τ. In particular, we know that the dynamical exponent z depends on both ρ and τ in the noninteracting limit, for the Aubry-André model [28]. If we make other choices of ρ and τ, is the charge gap scaling also independent on the remaining Hamiltonian parameters, as long as we are at the critical point? Since this is a question that we can already ask in the noninteracting limit, we will take the class of models considered in the main text, in the noninteracting limit, with Hamiltonian given by:

$$H = -\sum_i c_i^\dagger c_{i+1} + t_2 \sum_i c_i^\dagger c_{i+2} + \text{H.c.} + \sum_i (V \cos(2\pi\tau_c i + \phi) + V_2 \cos[2(2\pi\tau_c i + \phi)]) c_i^\dagger c_i. \tag{F1}$$

For the finite-size scaling results that follow, we use open boundary conditions and the sizes and rational approximants τ_c given in Table II. The results are given in Fig. 17, where we can see that the scalings obtained at critical points of widely different models are very compatible for fixed ρ and τ. In

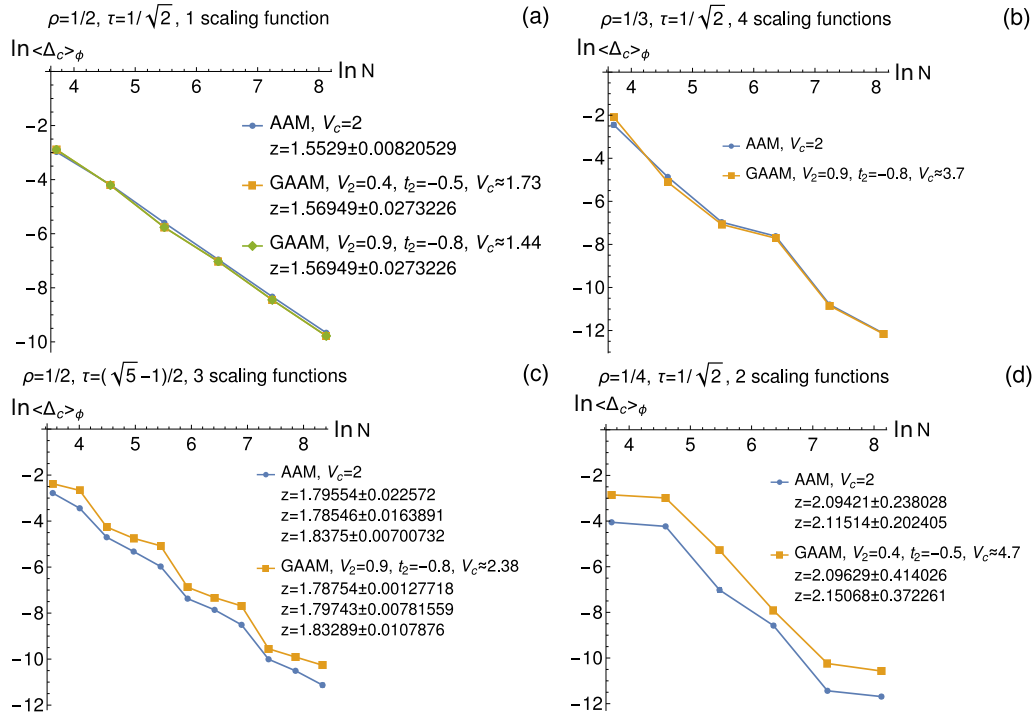

FIG. 17. Scaling of the charge gap using open boundary conditions and averaged over ϕ, for different fillings and choices of τ and at critical points of different models. The different critical points were estimated by imposing twisted boundary conditions and estimating the value $V = V_c$ for which $\Delta E_{\kappa\varphi} = 1$ (leaving the remaining parameters fixed), for the largest used system size. We indicate all the relevant parameters in the figure and also the number of scaling functions for the selected τ and ρ, that were obtained in Ref. [28]. The values of z indicated are extracted from fits using sizes $N_{\mathcal{N}j+1}$, $j = 0, \ldots, j_{\max}$ of the lists given in Table II, where $\mathcal{N}$ is the number of scaling functions. In (a) we used the five largest sizes, in (c) the three largest sizes belonging to each scaling function and in (d) we used all sizes. The different z estimates in (c), (d) for the same critical points were obtained from fits to sizes that belong to the different existing scaling functions.

some cases, there are more than one scaling functions, which means that an accurate finite-size scaling analysis should consider the system sizes that belong to the different scaling functions separately [28]. Remarkably, even the scaling features that arise due to the existence of multiple scaling functions (e.g., the three-step scaling in Fig. 17 due to the existence of three scaling functions) holds at different critical points as long as ρ and τ are fixed. These results support our claim that the scaling invariance that we observed at the critical point is not a special feature of our choice of ρ and τ. We checked for additional models, e.g., the model in Ref. [34], and obtained compatible results.

[1] D. J. Boers, B. Goedeke, D. Hinrichs, and M. Holthaus, Phys. Rev. A **75**, 063404 (2007).

[2] G. Roati, C. D'Errico, L. Fallani, M. Fattori, C. Fort, M. Zaccanti, G. Modugno, M. Modugno, and M. Inguscio, Nature (London) **453**, 895 (2008).

[3] M. Modugno, New J. Phys. **11**, 033023 (2009).

[4] M. Schreiber, S. S. Hodgman, P. Bordia, H. P. Lüschen, M. H. Fischer, R. Vosk, E. Altman, U. Schneider, and I. Bloch, Science **349**, 842 (2015).

[5] H. P. Lüschen, S. Scherg, T. Kohlert, M. Schreiber, P. Bordia, X. Li, S. Das Sarma, and I. Bloch, Phys. Rev. Lett. **120**, 160404 (2018).

[6] H. Yao, A. Khoudli, L. Bresque, and L. Sanchez-Palencia, Phys. Rev. Lett. **123**, 070405 (2019).

[7] H. Yao, T. Giamarchi, and L. Sanchez-Palencia, Phys. Rev. Lett. **125**, 060401 (2020).

[8] R. Gautier, H. Yao, and L. Sanchez-Palencia, Phys. Rev. Lett. **126**, 110401 (2021).

[9] F. A. An, K. Padavić, E. J. Meier, S. Hegde, S. Ganeshan, J. H. Pixley, S. Vishveshwara, and B. Gadway, Phys. Rev. Lett. **126**, 040603 (2021).

[10] T. Kohlert, S. Scherg, X. Li, H. P. Lüschen, S. Das Sarma, I. Bloch, and M. Aidelsburger, Phys. Rev. Lett. **122**, 170403 (2019).

[11] L. Balents, C. R. Dean, D. K. Efetov, and A. F. Young, Nature Phys. **16**, 725 (2020).

[12] V. Khemani, D. N. Sheng, and D. A. Huse, Phys. Rev. Lett. **119**, 075702 (2017).

[13] F. Setiawan, D.-L. Deng, and J. H. Pixley, Phys. Rev. B **96**, 104205 (2017).

[14] A. Chandran and C. R. Laumann, Phys. Rev. X **7**, 031061 (2017).

[15] U. Agrawal, S. Gopalakrishnan, and R. Vasseur, Nature Commun. **11**, 2225 (2020).

[16] S. Iyer, V. Oganesyan, G. Refael, and D. A. Huse, Phys. Rev. B **87**, 134202 (2013).

[17] R. Mondaini and M. Rigol, Phys. Rev. A **92**, 041601(R) (2015).
[18] R. Modak and S. Mukerjee, Phys. Rev. Lett. **115**, 230401 (2015).
[19] M. Lee, T. R. Look, S. P. Lim, and D. N. Sheng, Phys. Rev. B **96**, 075146 (2017).
[20] M. Žnidarič and M. Ljubotina, Proc. Natl. Acad. Sci. **115**, 4595 (2018).
[21] S. Xu, X. Li, Y.-T. Hsu, B. Swingle, and S. Das Sarma, Phys. Rev. Res. **1**, 032039(R) (2019).
[22] E. V. H. Doggen and A. D. Mirlin, Phys. Rev. B **100**, 104203 (2019).
[23] D. D. Vu, K. Huang, X. Li, and S. Das Sarma, Phys. Rev. Lett. **128**, 146601 (2022).
[24] A. S. Aramthottil, T. Chanda, P. Sierant, and J. Zakrzewski, Phys. Rev. B **104**, 214201 (2021).
[25] S. Aubry and G. André, Proceedings, VIII International Colloquium on Group-Theoretical Methods in Physics 3, 1980.
[26] A. Avila and S. Jitomirskaya, in *Mathematical Physics of Quantum Mechanics* (Springer, Berlin, 2006), pp. 5–16
[27] A. Szabó and U. Schneider, Phys. Rev. B **98**, 134201 (2018).
[28] T. Cookmeyer, J. Motruk, and J. E. Moore, Phys. Rev. B **101**, 174203 (2020).
[29] M. Johansson and R. Riklund, Phys. Rev. B **43**, 13468 (1991).
[30] J. Biddle and S. Das Sarma, Phys. Rev. Lett. **104**, 070601 (2010).
[31] J. D. Bodyfelt, D. Leykam, C. Danieli, X. Yu, and S. Flach, Phys. Rev. Lett. **113**, 236403 (2014).
[32] F. Liu, S. Ghosh, and Y. D. Chong, Phys. Rev. B **91**, 014108 (2015).
[33] C. Danieli, J. D. Bodyfelt, and S. Flach, Phys. Rev. B **91**, 235134 (2015).
[34] S. Ganeshan, J. H. Pixley, and S. Das Sarma, Phys. Rev. Lett. **114**, 146601 (2015).
[35] T. Liu, X. Xia, S. Longhi, and L. Sanchez-Palencia, SciPost Phys. **12**, 027 (2022).
[36] J. Vidal, D. Mouhanna, and T. Giamarchi, Phys. Rev. Lett. **83**, 3908 (1999).
[37] C. Schuster, R. A. Römer, and M. Schreiber, Phys. Rev. B **65**, 115114 (2002).
[38] G. Roux, T. Barthel, I. P. McCulloch, C. Kollath, U. Schollwöck, and T. Giamarchi, Phys. Rev. A **78**, 023628 (2008).
[39] Y. E. Kraus, O. Zilberberg, and R. Berkovits, Phys. Rev. B **89**, 161106(R) (2014).
[40] P. Naldesi, E. Ercolessi, and T. Roscilde, SciPost Phys. **1**, 010 (2016).
[41] D. D. Vu and S. Das Sarma, Phys. Rev. Lett. **126**, 036803 (2021).
[42] P. J. D. Crowley, A. Chandran, and C. R. Laumann, Phys. Rev. Lett. **120**, 175702 (2018).
[43] P. J. D. Crowley, C. R. Laumann, and A. Chandran, J. Stat. Mech.: Theory Exp. (2022) 083102.
[44] D. D. Vu and S. Das Sarma, Phys. Rev. B **106**, L121103 (2022).
[45] V. Mastropietro, Commun. Math. Phys. **351**, 283 (2017).
[46] J. Vidal, D. Mouhanna, and T. Giamarchi, Phys. Rev. B **65**, 014201 (2001).
[47] B.-B. Wei, Phys. Rev. A **99**, 042117 (2019).
[48] M. Gonçalves, B. Amorim, E. V. Castro, and P. Ribeiro, SciPost Phys. **13**, 046 (2022).
[49] R. Resta and S. Sorella, Phys. Rev. Lett. **82**, 370 (1999).
[50] R. Resta, Eur. Phys. J. B **79**, 121 (2011).
[51] V. Kerala Varma and S. Pilati, Phys. Rev. B **92**, 134207 (2015).
[52] M. Gonçalves, B. Amorim, E. V. Castro, and P. Ribeiro, Phys. Rev. B **108**, L100201 (2023).
[53] S. R. White, Phys. Rev. Lett. **69**, 2863 (1992).
[54] U. Schollwöck, Rev. Mod. Phys. **77**, 259 (2005).
[55] M. Fishman, S. R. White, and E. M. Stoudenmire, The ITensor software library for tensor network calculations, SciPost Phys. Codebases, 4 (2022).
[56] M. Fishman, S. R. White, and E. M. Stoudenmire, Codebase release 0.3 for ITensor, SciPost Phys. Codebases 4-r0.3 (2022).
[57] R. Resta, J. Phys.: Condens. Matter **30**, 414001 (2018).
[58] G. Vidal, J. I. Latorre, E. Rico, and A. Kitaev, Phys. Rev. Lett. **90**, 227902 (2003).
[59] L. Amico, R. Fazio, A. Osterloh, and V. Vedral, Rev. Mod. Phys. **80**, 517 (2008).
[60] P. Calabrese and J. Cardy, J. Stat. Mech.: Theory Exp. (2004) P06002.
[61] S. Ejima, F. Gebhard, and S. Nishimoto, Europhys. Lett. **70**, 492 (2005).
[62] R. T. Clay, A. W. Sandvik, and D. K. Campbell, Phys. Rev. B **59**, 4665 (1999).
[63] S. Ejima and H. Fehske, Europhys. Lett. **87**, 27001 (2009).
[64] R. T. Clay and R. P. Hardikar, Phys. Rev. Lett. **95**, 096401 (2005).
[65] F. Evers and A. D. Mirlin, Rev. Mod. Phys. **80**, 1355 (2008).
[66] C. Aulbach, A. Wobst, G.-L. Ingold, P. Hänggi, and I. Varga, New J. Phys. **6**, 70 (2004).
[67] P. Ribeiro, M. Haque, and A. Lazarides, Phys. Rev. A **87**, 043635 (2013).
[68] F. Iglói, R. Juhász, and Z. Zimborás, Europhys. Lett. **79**, 37001 (2007).
[69] G. m. H. Roósz, Z. Zimborás, and R. Juhász, Phys. Rev. B **102**, 064204 (2020).
[70] J. T. Chalker and G. J. Daniell, Phys. Rev. Lett. **61**, 593 (1988).
[71] J. Chalker, Physica A **167**, 253 (1990).
[72] E. Cuevas and V. E. Kravtsov, Phys. Rev. B **76**, 235119 (2007).
[73] M. S. Foster, H.-Y. Xie, and Y.-Z. Chou, Phys. Rev. B **89**, 155140 (2014).
[74] Y.-Z. Chou, Y. Fu, J. H. Wilson, E. J. König, and J. H. Pixley, Phys. Rev. B **101**, 235121 (2020).
[75] E. Abrahams, P. W. Anderson, D. C. Licciardello, and T. V. Ramakrishnan, Phys. Rev. Lett. **42**, 673 (1979).
[76] T. Giamarchi and H. J. Schulz, Phys. Rev. B **37**, 325 (1988).
[77] P. Schmitteckert, T. Schulze, C. Schuster, P. Schwab, and U. Eckern, Phys. Rev. Lett. **80**, 560 (1998).
[78] E. V. H. Doggen, G. Lemarié, S. Capponi, and N. Laflorencie, Phys. Rev. B **96**, 180202(R) (2017).
[79] S.-H. Lin, B. Sbierski, F. Dorfner, C. Karrasch, and F. Heidrich-Meisner, SciPost Phys. **4**, 002 (2018).
[80] R. Berkovits, Phys. Rev. Lett. **115**, 206401 (2015).
[81] Z. Ristivojevic, A. Petković, P. Le Doussal, and T. Giamarchi, Phys. Rev. Lett. **109**, 026402 (2012).
[82] E. Altman, Y. Kafri, A. Polkovnikov, and G. Refael, Phys. Rev. B **81**, 174528 (2010).
[83] L. Pollet, N. V. Prokof'ev, and B. V. Svistunov, Phys. Rev. B **89**, 054204 (2014).

[84] L. Pollet, N. V. Prokof'ev, B. V. Svistunov, and M. Troyer, Phys. Rev. Lett. **103**, 140402 (2009).
[85] B. Damski, J. Zakrzewski, L. Santos, P. Zoller, and M. Lewenstein, Phys. Rev. Lett. **91**, 080403 (2003).
[86] R. Roth and K. Burnett, Phys. Rev. A **68**, 023604 (2003).
[87] T. Roscilde, Phys. Rev. A **77**, 063605 (2008).
[88] X. Deng, R. Citro, A. Minguzzi, and E. Orignac, Phys. Rev. A **78**, 013625 (2008).
[89] M. Gonçalves, B. Amorim, E. V. Castro, and P. Ribeiro, Critical phase dualities in 1D exactly solvable quasiperiodic models, Phys. Rev. Lett., **131**, 186303 (2023).
[90] S. Ostlund, R. Pandit, D. Rand, H. J. Schellnhuber, and E. D. Siggia, Phys. Rev. Lett. **50**, 1873 (1983).
[91] A. Jagannathan, Rev. Mod. Phys. **93**, 045001 (2021).
[92] M. Gonçalves, B. Amorim, F. Riche, E. V. Castro, and P. Ribeiro, arXiv:2305.03800 [cond-mat.str-el].
[93] Z. Fan, G.-W. Chern, and S.-Z. Lin, Phys. Rev. Res. **3**, 023195 (2021).
[94] X. Zhang and M. S. Foster, Phys. Rev. B **106**, L180503 (2022).
[95] R. Oliveira, M. Gonçalves, P. Ribeiro, E. V. Castro, and B. Amorim, arXiv:2303.17656 [cond-mat.supr-con].
[96] M. V. Feigel'man, L. B. Ioffe, V. E. Kravtsov, and E. A. Yuzbashyan, Phys. Rev. Lett. **98**, 027001 (2007).
[97] K. Zhao, H. Lin, X. Xiao, W. Huang, W. Yao, M. Yan, Y. Xing, Q. Zhang, Z.-X. Li, S. Hoshino, J. Wang, S. Zhou, L. Gu, M. S. Bahramy, H. Yao, N. Nagaosa, Q.-K. Xue, K. T. Law, X. Chen, and S.-H. Ji, Nature Phys. **15**, 904 (2019).
[98] T. C. Wu, P. A. Lee, and M. S. Foster, Enhancement of superconductivity in a dirty marginal Fermi liquid, Phys. Rev. B, **108**, 214506 (2023).
[99] J. F. Karcher, M. Sonner, and A. D. Mirlin, Phys. Rev. B **100**, 134207 (2019).
[100] T. P. Eggarter and R. Riedinger, Phys. Rev. B **18**, 569 (1978).
[101] O. Motrunich, K. Damle, and D. A. Huse, Phys. Rev. B **63**, 134424 (2001).
[102] M. Gonçalves, P. Ribeiro, and I. M. Khaymovich, Phys. Rev. B **108**, 104201 (2023).